Structural basis for regulation of Frizzled-4 signaling by the co-receptor Tetraspanin-12

Alyana J. Granados[1,3], Payal P. Pratap[1,3], Kevin Alexander Estrada Alamo[1,2], Katherine J. Susa[1,†]

[1] Department of Pharmaceutical Chemistry, University of California, San Francisco, CA 94158, USA

[2] Program in Biophysics, University of California, San Francisco, CA 94158, USA

[3] These authors contributed equally.

[†]Correspondence and requests for materials should be sent to Katherine J. Susa (Katherine.Susa@ucsf.edu)

ABSTRACT

Norrin is an atypical ligand that regulates retinal angiogenesis through the Wnt/β-catenin pathway. Norrin triggers heterodimerization of Frizzled-4 (FZD4) with Low-density lipoprotein receptor-related protein 5 or 6 (LRP5/6), leading to downstream β-catenin stabilization. Unlike Wnt ligands, Norrin requires the tetraspanin Tspan12 for signaling amplification, but it is not understood why. Here, we report a 3.4-angstrom structure of Tspan12 in complex with FZD4 determined by cryo-electron microscopy. The structure reveals that FZD4 and Tspan12 form a direct complex in the absence of Norrin. The transmembrane (TM) domain of Tspan12 is oriented in a tightly packed four-helix bundle and interacts with TM2 of FZD4 to promote trafficking of Tspan12 to the cell surface. The C-D helices of Tspan12, which mediate binding to Norrin, remain exposed while Tspan12 is in complex with FZD4, facilitating higher-affinity Norrin binding. Cell-based assays reveal that Tspan12 and FZD4 remain associated after Norrin recognition, suggesting that Tspan12 is a core component of the FZD4-Norrin-LRP5/6 signaling complex. Together, these studies reveal the molecular mechanism underlying the assembly of the Tspan12-FZD4 complex and the enhancement of Norrin signaling, suggesting new ways to target the FZD4-Tspan12 complex for ocular diseases characterized by hypo- or hyper-vascularization.

SIGNIFICANCE STATEMENT

Blood vessel formation in the retina is essential for vision, and its disruption leads to ocular diseases. Norrin regulates retinal angiogenesis by triggering the heterodimerization of Frizzled-4 with co-receptor LRP5/6, mimicking the function of Wnt ligands and leading to downstream β-catenin signaling. Unlike Wnts, Norrin requires a tetraspanin family member, Tspan12, to amplify signaling. We report the structure of the FZD4-Tspan12 co-receptor complex and identify key interacting regions that enable Tspan12 trafficking to the cell surface and higher affinity capture of Norrin. Cell-based assays indicate Tspan12 remains a component of the active Norrin-FZD4-LRP5/6 signaling complex. Our results highlight an underappreciated role of tetraspanins in direct

regulation of receptor signaling and suggest new therapeutic avenues for targeting abnormalities in vascular growth.

127 **INTRODUCTION**
128
129 Wnt/β-catenin signaling is a highly conserved cellular communication pathway that is one
130 of the main regulators of development, cell fate determination, tissue homeostasis, and tissue
131 regeneration in metazoans (1). Wnts, a family of secreted, lipid-modified growth factors, initiate
132 signaling by binding to G-protein coupled receptors (GPCRs) of the Frizzled family, which contain
133 an extracellular N-terminal cysteine-rich domain (CRD) (2, 3). Wnt binding within the CRD (4, 5)
134 promotes heterodimer formation with the co-receptor Low-density lipoprotein receptor-related
135 protein 5 or 6 (LRP5/6)(6). FZD-LRP5/6 heterodimers recruit the intracellular signaling effectors
136 Dishevelled (Dvl) (7) and Axin (8), ultimately leading to stabilization of the transcriptional co-
137 activator β-catenin and induction of Wnt target genes to drive cell division, migration, and
138 differentiation (9). In line with this, dysregulated signaling can lead to developmental defects,
139 cancer, and degenerative disorders (1, 10).
140 In the early 1990s, an atypical ligand that activates β-catenin signaling, Norrin (Norrie
141 Disease Protein, NDP), was discovered through experiments aimed at identifying genes
142 associated with Norrie disease, a neurodevelopmental disorder characterized by severe vision
143 loss or blindness, intellectual disability, and hearing loss (11, 12). Norrin has a transforming
144 growth factor-β-like cysteine knot fold and is homodimeric, consisting of two disulfide-linked
145 protomers (13). Norrin has no structural homology to Wnts yet mimics their function. Each Norrin
146 protomer contains non-overlapping binding sites for the CRD of FZD4 and for LRP5/6, which
147 triggers heterodimerization of FZD with LRP5/6 to initiate β-catenin signaling (14). Unlike Wnt
148 ligands, which bind promiscuously to multiple FZD family members (15), Norrin specifically binds
149 to FZD4 out of the ten human Frizzled receptors (16). Norrin/FZD4 signaling is essential for retinal
150 blood vessel formation and blood-retina barrier development (17). Consistent with this critical role,
151 mutations in genes encoding components of this pathway—including Norrin, FZD4, and LRP5—
152 cause familial exudative vitreoretinopathy (FEVR), a hereditary ocular disorder related to Norrie
153 disease characterized by retinal hypo-vascularization, leading to retinal detachment, vision loss,

154 or blindness (18, 19). Additionally, Norrin plays important roles in angiogenesis not only for eye
155 development but also in the ear, brain, and female reproductive system (13).

156 Compared to Wnt ligands, Norrin has the unique feature of utilizing a member of the
157 tetraspanin family as a co-receptor to amplify β-catenin signaling. Nearly two decades after the
158 identification of Norrin, a large-scale reverse genetic screen revealed that mutations in the gene
159 encoding for Tetraspanin-12 (Tspan12) mimic the retinal vascular defects of NDP, FZD4, and
160 LRP5 mutant mice (20).Tspan12 is a member of the ancient, highly conserved tetraspanin family
161 of four-pass transmembrane proteins, which have been termed “molecular facilitators” (21).
162 Tetraspanins bind transmembrane partner proteins to regulate a range of fundamental signal
163 transduction pathways (22, 23), including B cell (24, 25), Notch (26), and integrin (27, 28) signaling
164 through regulation of partner protein trafficking and membrane microdomain localization. Cell-
165 based assays demonstrated that Tspan12 functions as a co-receptor to significantly increase
166 Norrin/β-catenin signaling by about 4-fold, with no effect on Wnt/β-catenin signaling (20). In line
167 with Tspan12’s important role in amplifying Norrin signaling, mutations in Tspan12 cause FEVR
168 and account for approximately 5-10% of FEVR cases in humans (18, 19, 29–33).

169 The mechanism underlying Tspan12’s enhancement of FZD4 signaling has remained
170 unclear, with proposed models including the allosteric modulation of FZD4 to amplify signaling
171 (34), the promotion of FZD4 clustering (35), or the enhancement of FZD4/LRP5
172 heterodimerization (36). Tspan12 can rescue β-catenin signaling disrupted by point mutations
173 that impair the Norrin-FZD4 interaction, indicating that Tspan12 may enhance the binding of
174 Norrin to FZD4 (34). However, it is unclear whether Tspan12 achieves this function through a
175 direct interaction with FZD4. Recent biophysical experiments showed that Tspan12 directly binds
176 Norrin with high affinity (10 nM), and can bind to the same protomer of Norrin as the CRD of FZD4
177 (37). However, Tspan12 is competitive with LRP6 for binding to the same site on Norrin (37).
178 These data support a ligand hand-off mechanism, in which Tspan12 initially promotes the capture
179 of Norrin and then passes it off to FZD4 and LRP5/6 (37). An alternative mechanism is Tspan12

180 remaining incorporated in the Norrin-FZD4-LRP5/6 complex, with Tspan12 and LRP5/6 each
181 binding to separate protomers of Norrin. However, the structural basis for Tspan12 engaging a
182 single protomer remains unclear.

183 To understand how Tspan12 mediates enhancement of Norrin signaling, we determined
184 the structure of Tspan12 bound to FZD4 using single-particle cryo-electron microscopy (cryo-EM).
185 We then used cell-based signaling assays to characterize how Norrin binds to the Tspan12-FZD4
186 complex and monitor the dynamics of Tspan12-FZD4 upon Norrin recognition. Our structural
187 analysis and cell-based assays define the molecular basis for Tspan12 enhancement of Norrin
188 signaling and suggest a model in which Tspan12 does not "hand off" Norrin to FZD4 and LRP5
189 but instead remains associated as a constitutive component of the FZD4-LRP5/6 signaling
190 complex.

191
192 **RESULTS**
193
194 **Engineering and structure determination of the Tspan12-FZD4 complex**

195 Tspan12 requires interaction with FZD4 for trafficking to the cell surface (34) and co-
196 localizes with FZD4 on the cell surface (13, 34, 35), suggesting a direct interaction that initiates
197 in the endoplasmic reticulum (34). However, our initial attempts to purify a stable Tspan12-FZD4
198 complex through co-expression and dual-affinity tag purification were unsuccessful, likely due to
199 weak affinity between Tspan12-FZD4, which is consistent with prior reports for both Tspan12-
200 FZD4 and other tetraspanin-partner complexes (37, 38). To overcome this, we engineered a
201 construct with Tspan12 tethered to FZD4 to increase their local concentration and apparent
202 affinity. This construct contains the full-length FZD4 sequence connected to full-length Tspan12
203 with a flexible glycine-glycine-serine (GGS) linker **(Supplementary Figure 1A)**.

204 To validate that this tethered construct maintains the natural interaction that facilitates
205 FZD4-mediated trafficking of Tspan12 to the cell surface, we used a flow cytometry-based
206 trafficking assay to monitor Tspan12 surface expression with an anti-Tspan12 antibody **(Figure**

207 **1A)**. While Tspan12 expressed alone showed low levels on the cell surface, co-expression with
208 FZD4 resulted in a 4-fold increase in Tspan12 trafficking to the cell surface **(Figure 1A)**. The
209 tethered Tspan12-FZD4 construct displayed a similar magnitude of increase in Tspan12 surface
210 trafficking as Tspan12 co-transfected with FZD4, indicating that our engineered construct retains
211 the interaction that mediates Tspan12 trafficking and is properly folded **(Figure 1A)**.

212 Initial structure determination efforts for the Tspan12-FZD4 complex by single particle
213 cryo-EM were unsuccessful due to the relatively small size of the complex (93 kDa) and limited
214 rigid extracellular features outside of the detergent micelle. To overcome this, we introduced the
215 thermostabilized BRIL domain (cytochrome b652 RIL) into intracellular loop 3 (ICL3) of FZD4,
216 following previously reported successful structure determination of inactive state GPCRs that
217 used an anti-BRIL Fab (BAG2) as a rigid fiducial marker to improve particle alignments (39, 40).
218 To optimize a rigid connection between FZD4 and BRIL, we used AlphaFold3 to guide linker
219 selection, choosing a linker that was predicted to form a continuous rigid helix with high confidence
220 **(Supplementary Figure 1B-D)** (41). We confirmed that the tethered FZD4-BRIL-Tspan12
221 construct maintained the ability to traffic Tspan12 to the cell surface. Our BRIL-engineered
222 construct resulted in enhanced levels of Tspan12 and FZD4 on the cell surface **(Supplementary**
223 **Figure 1E, F)**, indicating that the BRIL domain likely stabilizes FZD4, leading to higher expression
224 levels, which is consistent with prior reports (42).

225 For structure determination, we incubated purified FZD4-BRIL-Tspan12 with anti-BRIL
226 Fab (43) and an anti-Fab nanobody (44) **(Supplementary Figure 1G, H)**. Cryo-EM imaging of
227 this complex revealed well-dispersed particles, and two-dimensional class averages showed clear
228 secondary structures in both the Fab region and transmembrane region **(Supplementary Figure**
229 **2)**. Subsequent 3D refinement resulted in a structure of FZD4-BRIL-Tspan12 bound to the anti-
230 BRIL F_{ab} and anti-F_{ab} nanobody at an overall nominal resolution of 3.4 Å, with density well defined
231 for all features of the complex, except the N-terminal CRD-Hinge region of FZD4 and the C-
232 terminal tail of Tspan12, both of which are highly flexible **(Figure 1B, Supplementary Table 1)**.

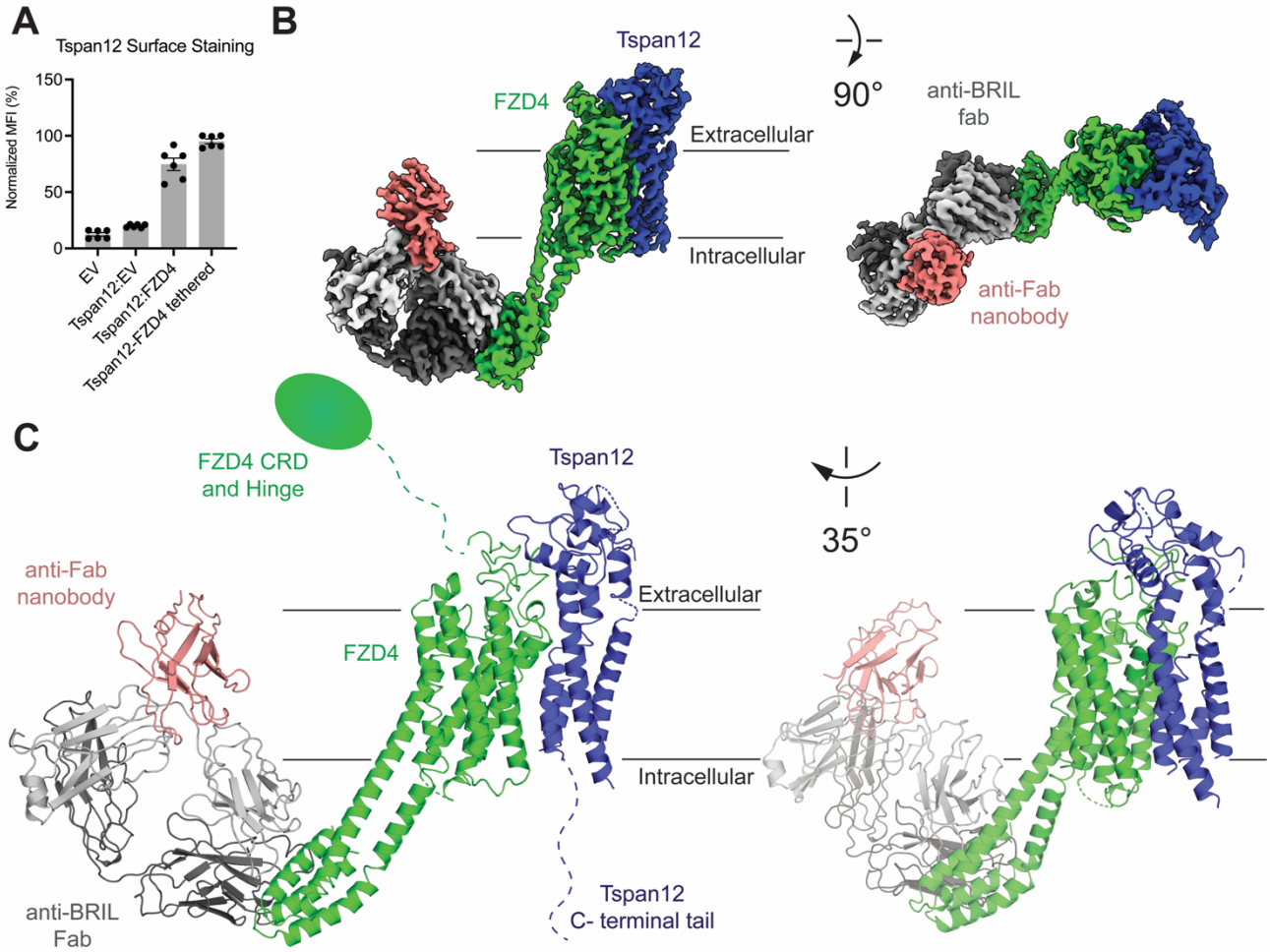

Figure 1: 3D reconstruction and atomic model of the human FZD4-Tspan12 complex bound to an anti-BRIL F_{ab} and anti-F_{ab} nanobody (PDB: 9YEV). (A) Tspan12 trafficking assay with Tspan12 either transfected with empty vector (EV), FZD4, or as a tethered complex with FZD4. Surface Tspan12 was detected by flow cytometry using an Alexa 647-coupled anti-Tspan12 antibody (Biotechne FAB8910R-025). **(B)** Different views of the cryo-EM map of the FZD4-Tspan12-anti-BRIL F_{ab}-anti-F_{ab} nanobody complex, colored by subunit. **(C)** Ribbon representation of the structure of the complex. FZD4, Tspan12, the anti-F_{ab} nanobody, and the anti-BRIL F_{ab} are colored as in B. In Panel A, error bars represent mean ± SEM of two independent experiments, with three technical replicates each.

Tspan12 does not alter FZD4 conformation

To build the initial model, AlphaFold3 (45) models of FZD4-BRIL and Tspan12, along with the structures of the anti-BRIL-F_{ab} and anti-F_{ab} nanobodies (39), were docked into the cryo-EM

density map and manually rebuilt. While the FZD4 model fit readily into the density map, the transmembrane helices of Tspan12 had to be separately docked due to differences in their orientation compared to the AlphaFold3 model **(Supplementary Figure 3)**. In the complex, Tspan12 packs against the second and third transmembrane domains (TM2 and TM3) of FZD4 via hydrophobic interactions and also makes contacts with extracellular loop 1 (ECL1) and the lower region of the hinge domain (also termed "linker") of FZD4, which is a flexible region connecting the CRD to the 7-transmembrane domain (40, 46) **(Figure 1C, Supplementary Figure 3B-D)**. The FZD4-Tspan12 complex buries a total of approximately 1338 $Å^2$ at the interface between the ectodomains and transmembrane domains.

One model of Tspan12 enhancement of signaling is that Tspan12 allosterically activates FZD4 to enhance binding of the intracellular signaling effector Dvl (34). However, recent experiments have shown that the affinity of the Dvl2 DEP domain for the Tspan12-FZD4 complex is not significantly different than its affinity for Fzd4 alone (37). In line with this, the FZD4-Tspan12 structure shows no change in FZD4 conformation compared to the inactive state crystal structure of FZD4 (PDB: 6BD4), with a root mean square deviation (RMSD) of 0.68 Å **(Supplementary Figure 4A)**, indicating that Tspan12 is not functioning to allosterically activate FZD4 (47). A structure of FZD4 bound to the DEP domain of Dvl2 was also determined by cryo-EM (PDB: 8WMA), which revealed that DEP induces a subtle outward movement of TM6 (4.0 Å) and a slight inward movement of TM5 of FZD4 (48). Tspan12 binds to TM2 and TM3 of FZD4 and makes no contacts with FZD4 that would interfere with DEP engagement, indicating that Tspan12 can remain bound to FZD4 after Dvl engagement **(Supplementary Figure 4B)**. While it is possible that the BRIL fusion may influence these structural comparisons, our results indicate that it is unlikely that Tspan12 plays a significant allosteric role.

The C-D helices of Tspan12 are exposed within the FZD4 complex to facilitate higher affinity Norrin binding

281 Tspan12 is the only known tetraspanin identified to date with an obvious receptor function
282 for an endogenous secreted ligand, binding to Norrin within its ectodomain with an affinity of
283 approximately 10 nM (34, 37, 49). In line with this, Tspan12 has a particularly unique mode of
284 engagement with FZD4 compared to other tetraspanin-partner structures solved to date **(Figure**
285 **2A and 2B)**. In addition to their four-pass transmembrane domain, tetraspanins have two
286 extracellular domains, a small extracellular loop (SEL) and a large extracellular loop (LEL) (23).
287 Within the LEL, tetraspanins have two hypervariable helices, the "C" and "D" helices. Among
288 different members of the tetraspanin family, these helices are highly variable in sequence and
289 structure, representing an important site where structural variability in tetraspanins encodes
290 specificity for their interactions with partners (23). Two other structures of tetraspanins with non-
291 tetraspanin partners have been reported to date at a resolution sufficient to build an atomic
292 model—the tetraspanin CD81 with the B cell co-receptor CD19, and Tspan15 with the
293 metalloprotease ADAM10 (38, 50). In both of these structures, the C and D helices form the
294 primary interaction interface with the partner protein. However, in the structure of Tspan12 bound
295 to FZD4, the C and D helices are completely exposed and highly dynamic, making up the area of
296 poorest local resolution in the cryo-EM map **(Supplementary Figure 5).** The C and D helices
297 were recently shown to be the site of Norrin binding to Tspan12 using a high-confidence
298 AlphaFold-Multimer prediction and model-guided point mutagenesis (37). We used a flow-
299 cytometry-based binding assay to measure the EC_{50} of Norrin binding to the FZD4-Tspan12
300 tethered construct with an E170K mutation in Helix D of Tspan12, which is predicted by the Norrin-
301 Tspan12 AlphaFold model to form a hydrogen bond with Serine 83 of Norrin (37). This construct
302 bound Norrin with a 2-fold decrease in apparent affinity, confirming the C and D helices of
303 Tspan12 mediate binding to Norrin within the context of the FZD4-Tspan12 complex **(Figure 2C)**.
304
305
306

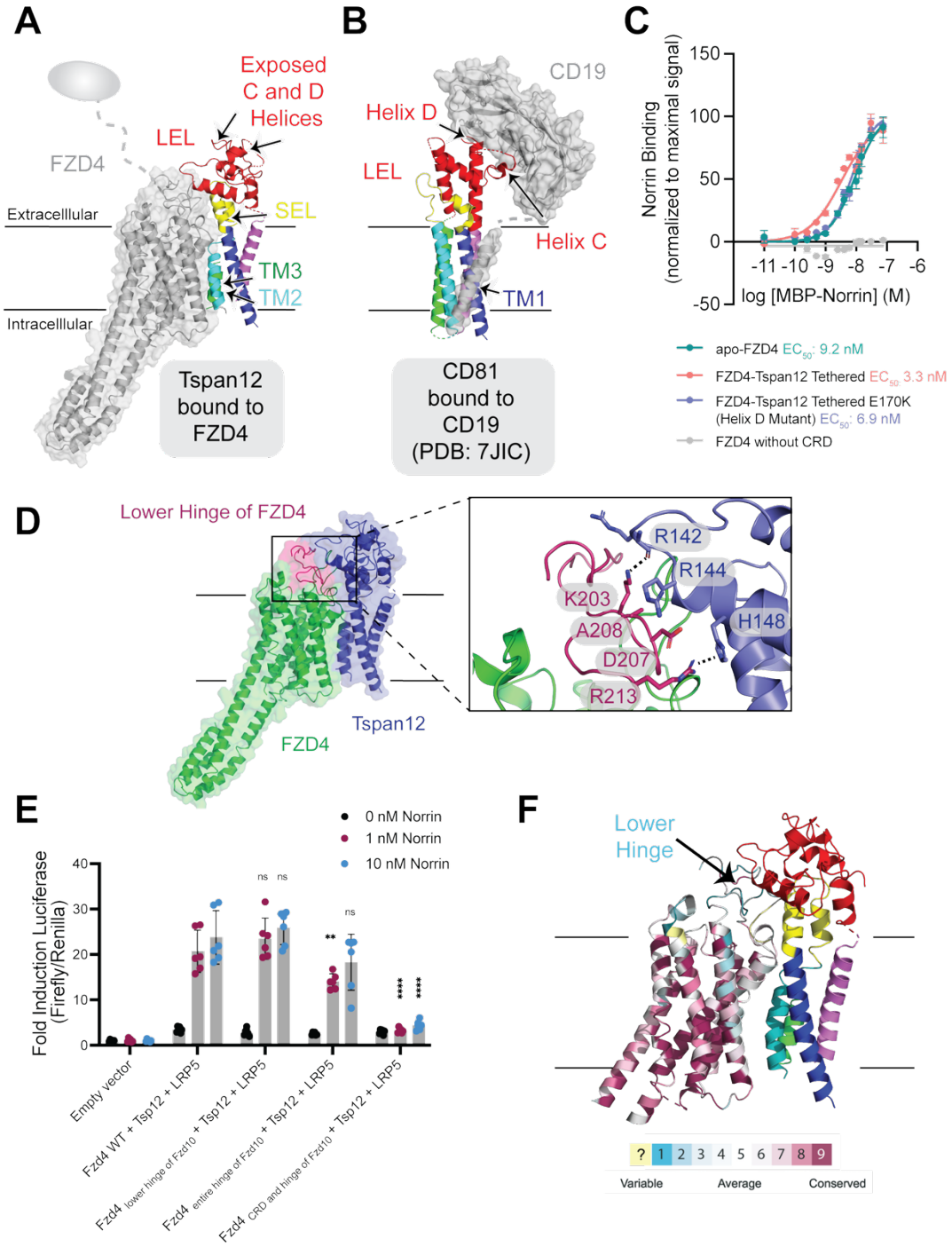

Figure 2: Characterization of Norrin binding to the FZD4-Tspan12 complex. (A and B) Comparison of the FZD4-Tspan12 complex to the CD19-CD81 (Tspan28) complex (PDB: 7JIC). The partner protein is colored in grey, and the tetraspanin is colored by domain. The tetraspanin CD81 utilizes the C-D helices within the LEL as the primary engagement site with its partner, CD19. In contrast, the structure of FZD4-Tspan12 shows that these two helices do not make contact with the partner. **(C)** Binding of Norrin to Expi293 cells expressing either apo-FZD4,

316 tethered FZD4-Tspan12, tethered FZD4-Tspan12 with an E170K point mutation in the D helix, or
317 FZD4 without the cysteine-rich domain (CRD) (negative control). Apo-FZD4 EC_{50}: 9.2 nM (95%
318 CI: 7.3 nM to 12.2 nM), Hill slope: 1.0 (95% CI: 0.9 to 1.2). Tethered FZD4-Tspan12 EC_{50}: 3.3 nM
319 (95% CI: 2.0 nM to 6.5 nM), Hill slope: 0.8 (95% CI: 0.6 to 1.1). Tethered FZD4-Tspan12 E170K
320 EC_{50}: 6.9 nM (95% CI: 6.0 nM to 8.4 nM), Hill slope: 1.1 (95% CI: 1.0 to 1.3). Experiments were
321 performed in triplicate with error bars representing mean ± SEM. In all binding experiments, FZD4
322 without the CRD was used as a control for background binding. **(D)** Interaction between the lower
323 hinge of FZD4 and Tspan12, showing a zoomed-in interface. **(E)** TOPFlash signaling assay with
324 FZD4/FZD10 chimeras with swaps in the lower hinge or entire hinge domain, or with the entire
325 CRD and hinge (negative control). Expression of chimeric FZD constructs is shown in
326 Supplementary Figure 6. Error bars represent mean ± SEM of two independent experiments, with
327 three technical replicates each. Statistical analysis was performed in GraphPad Prism using an
328 unpaired t-test, comparing wild-type FZD4:Tspan12:LRP5 to each corresponding Norrin
329 concentration of the chimeric FZD4:Tspan12:LRP5 conditions. *$p \leq 0.05$, **$p \leq 0.01$, ***$p \leq 0.001$,
330 ****$p \leq 0.0001$, ns: not significant. **(F)** Structure of FZD4-Tspan12, with FZD4 colored by residue
331 conservation among the 9 human Frizzled paralogs. Residues are colored on a sliding scale from
332 magenta (highly conserved) to blue (poorly conserved). Residues with insufficient information for
333 analysis are colored yellow. Conservation was determined using the Consurf server (51).
334
335
336
337 Tspan12 and FZD4 bind to non-overlapping regions on the same protomer of Norrin (37).
338 Because the C and D helices of Tspan12 remain accessible for Norrin capture when Tspan12 is
339 bound to FZD4, we hypothesized that this may provide avidity to promote increased Norrin
340 capture by positioning the CRD (the Norrin binding domain of FZD4) and the C-D helices of
341 Tspan12 in close proximity. To test this, we measured the EC_{50} of Norrin binding to the tethered
342 FZD4-Tspan12 construct compared to FZD4 alone using a flow cytometry-based binding assay.
343 The tethered construct bound Norrin with approximately 3-fold higher apparent affinity, with an
344 EC_{50} of 3.3 nM (95% confidence interval (CI): 2.0 nM to 6.5 nM) for the FZD4-Tspan12 complex
345 and 9.1 nM (95% CI: 7.3 nM to 12.2 nM) for apo-FZD4 **(Figure 2C)**. These data indicate that one
346 function of Tspan12 is to enable response to low Norrin concentrations.

347 **Tspan12 interacts with the lower hinge of FZD4**

348 The Tspan12-FZD4 structure revealed that the LEL of Tspan12 interacts with the lower
349 region of the hinge domain of FZD4 **(Figure 2D, Supplementary Figure 3B-C**). The hinge
350 domain connects the CRD to the 7-TM domain of FZD receptors. This domain is highly variable
351 in length and sequence among FZD family members and can be subdivided into a highly flexible

352 segment from the CRD to the first conserved cysteine residue, followed by a shorter, more
353 ordered segment from the first conserved cysteine to TM1 (40). While the CRD and upper hinge
354 segment are not observed in our structure due to inherent flexibility, a portion of the lower, ordered
355 hinge segment makes several contacts with the LEL of Tspan12. Within the hinge, Lysine 203 of
356 FZD4 hydrogen bonds with the carbonyl of Arginine 142 of Tspan12, and Arginine 213 of FZD4
357 interacts with Histidine 148 of Tspan12 **(Figure 2D, Supplementary Figure 3B-3C)**.

358 The hinge domain of FZD4 has been demonstrated to play a role in signaling. Swapping
359 the FZD4 hinge with the FZD5 hinge results in a loss of Norrin signaling and a decrease in affinity
360 for Norrin (52). We next asked if Tspan12's interaction with the lower hinge region of FZD4
361 contributes to Norrin signaling. To test this, we created FZD4 chimeras in which either the entire
362 hinge domain or just the lower hinge of FZD4 is replaced with that of FZD10, and a negative
363 control chimera in which the entire CRD and hinge were replaced with that of FZD10, and
364 assessed their ability to signal in the TOPFlash β-catenin reporter assay **(Supplementary Table
365 2, Supplementary Figure 6A)**. As expected, the FZD4 chimera with the CRD and hinge swap
366 does not signal, and the FZD4 chimera with the entire hinge region swapped with that of FZD10
367 showed decreased signaling at low Norrin concentrations **(Figure 2E)**. However, the FZD4
368 chimera with the lower hinge swapped for that of FZD10 signaled comparably to wild-type FZD4
369 at all Norrin concentrations tested **(Figure 2D)**. The lower hinge domain is highly sequence
370 divergent among the ten human Frizzled receptors, suggesting that, though this region does not
371 have an apparent role in signaling, it may help drive the specificity of the interaction of Tspan12
372 with only FZD4 out of the ten receptors **(Figure 2F)**.

373
374 **Interactions within the transmembrane domain mediate Tspan12 trafficking to the cell
375 surface**
376
377 Tspan12 and FZD4 initiate their partnership in the secretory pathway, and Tspan12 is
378 dependent on FZD4 for proper trafficking to the cell surface (34). This is highly unusual for a

379 member of the tetraspanin family—in other tetraspanin-partner trafficking relationships studied to
380 date, the tetraspanin is responsible for promoting the trafficking of the partner to the cell surface
381 (53). For example, the tetraspanin CD81 promotes the trafficking of its partner, CD19, to the cell
382 surface by covering an exposed, highly hydrophobic patch within the CD19 ectodomain, thereby
383 enhancing the surface expression of properly folded CD19, with CD19 having no reciprocal effect
384 on CD81 expression (38, 54).

385 Next, we asked how FZD4 promotes trafficking of Tspan12 to the cell surface. We created
386 a panel of FZD4 chimeras with domain swaps in domains that interact with Tspan12 **(Figure 3A,**
387 **Supplementary Table 2, Supplementary Figure 7)**. We replaced either ECL1, TM2, TM3, the
388 lower hinge, or the entire hinge of FZD4 with that of FZD10 and used a flow cytometry-based
389 trafficking assay to monitor the ability of these constructs to support Tspan12 surface expression.
390 While Tspan12 expressed without FZD4 showed low levels on the cell surface, co-expression of
391 Tspan12 with FZD4 resulted in a 4-fold enhancement of Tspan12 expression on the cell surface
392 **(Figure 3B)**. While the ECL1, TM3, and hinge chimeras had no effect on Tspan12 trafficking,
393 replacement of TM2 with that of FZD10 significantly reduced the amount of Tspan12 on the cell
394 surface, indicating that the interaction of Tspan12 with TM2 of FZD4 is a determinant of trafficking
395 **(Figure 3B).** In addition to Tspan12 abundance on the plasma membrane, blotting whole cell
396 lysate of cells co-transfected with Tspan12 and either wild type FZD4 or chimeric constructs
397 confirmed that in the presence of the TM2 chimera, significantly less Tspan12 is present in the
398 cell, indicating that Tspan12 is either being made less efficiently or is rapidly degraded in the
399 presence of the TM2 swap chimera **(Supplementary Figure 8).** TM2 of FZD4 packs against the
400 SEL and TM2 and TM3 of Tspan12, stabilizing a highly bent region between TM2 and the SEL of
401 Tspan12 (**Figure 3C, Supplementary Figure 3C**). Tspan12 can bind to Norrin with high affinity
402 in the absence of FZD4 (37), but it cannot signal unless it is complexed with FZD4 (35). This
403 unusual trafficking relationship for a tetraspanin may have evolved to prevent apo-Tspan12 from

being expressed in high amounts on the cell surface. Apo-Tspan12 would be able to bind to Norrin, but when not complexed to FZD4, it could act as a “sink” for Norrin by binding ligand but not being in close enough proximity to FZD4 for efficient signaling.

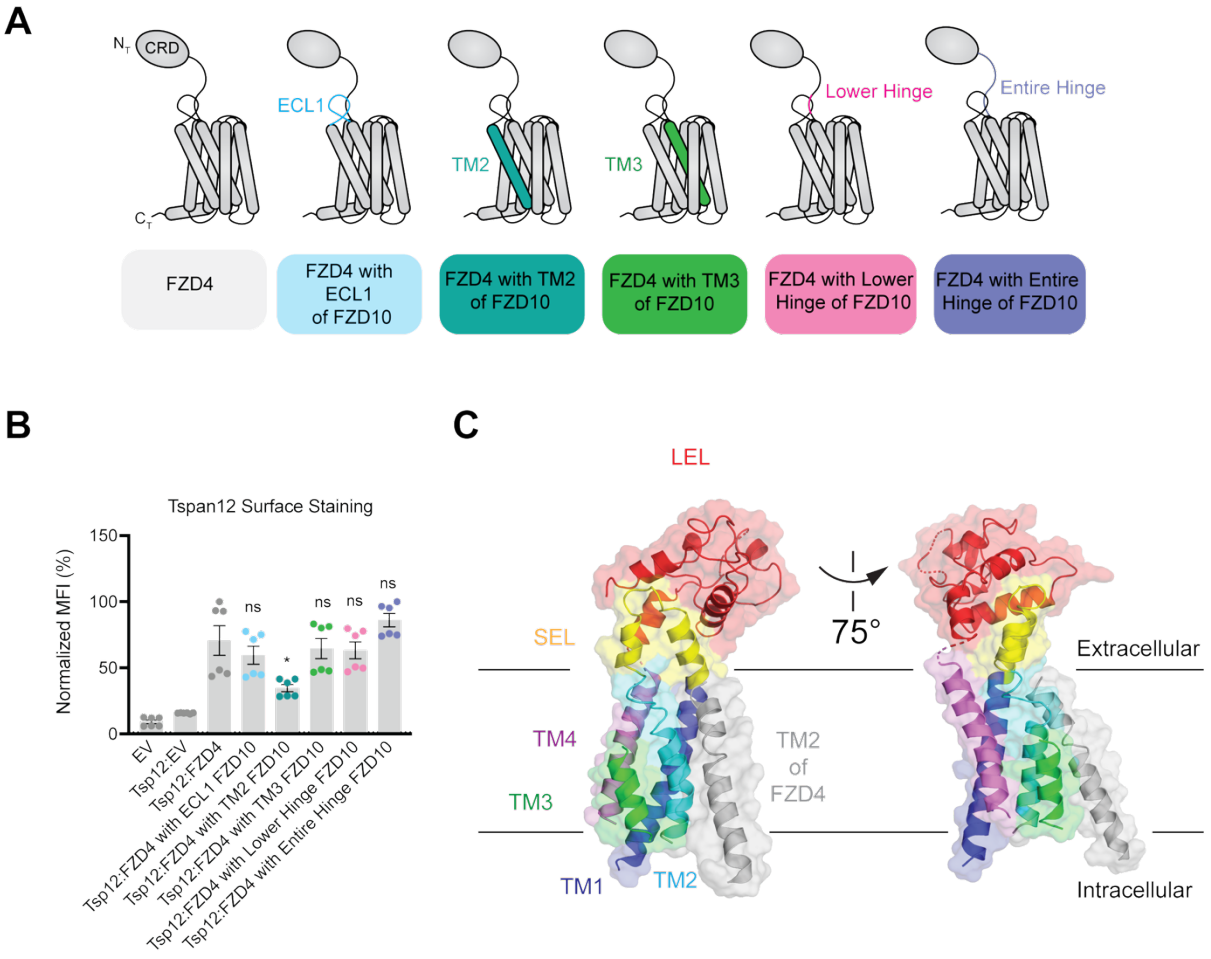

Figure 3: The second transmembrane domain of FZD4 is essential for Tspan12 trafficking to the cell surface. **(A)** Schematic of FZD4-FZD10 chimeras. ECL1, TM2, TM3, or the hinge of FZD4 was replaced with that of FZD10. **(B)** Tspan12 trafficking assay with Tspan12 co-transfected with empty vector (EV), FZD4, or a FZD4-FZD10 chimera. Surface Tspan12 was detected by flow cytometry using an Alexa 647-coupled anti-Tspan12 antibody (Biotechne FAB8910R-025). Error bars represent mean ± SEM of two independent experiments, with three technical replicates each. Statistical analysis was performed in GraphPad Prism using an unpaired t-test, comparing Tspan12:FZD4 to each Tspan12: chimeric FZD4 condition. *$p \leq 0.05$, **$p \leq 0.01$, ***$p \leq 0.001$, **** $p \leq 0.0001$. Expression of chimeric FZD constructs is shown in Supplementary Figure 7. **(C)** Atomic representation of Tspan12 bound to FZD4, colored by domain. TM2 of FZD4 (grey) packs against TM2, TM3, and the SEL of Tspan12.

421
422
423 **Dynamics of the FZD4-Tspan12 interaction**
424
425 A “hand-off” mechanism for Tspan12 function was proposed in which Tspan12 initially
426 promotes the capture of Norrin and then passes off Norrin to FZD4 and LRP5/6, leading to
427 downstream signaling (37). This model is based on evidence that Tspan12 and LRP6 compete
428 for the same binding site on Norrin (37), suggesting that Tspan12 may dissociate from FZD4 after
429 Norrin recognition to facilitate LRP5/6 heterodimerization. We and others have previously shown
430 that tetraspanins are conformationally dynamic, switching between an “open” state (38) and a
431 “closed” state (55). The “open” conformation of the tetraspanin CD81 has a higher affinity for its
432 partner CD19 (38, 55, 56), and we hypothesized that conformational changes in Tspan12
433 between an open and closed state may facilitate dissociation from FZD4. While the “closed”
434 conformation has a cone-shaped orientation of the transmembrane helices and a large
435 hydrophobic binding pocket capable of binding lipids (55, 57), the “open” conformation has a
436 tightly packed four-helix bundle orientation of the TMs, which occludes the lipid binding pocket,
437 and is characterized by a hinge opening of the ectodomain away from the membrane (38, 58).
438 When bound to FZD4, Tspan12 is in the “open” conformation, with a tightly packed orientation of
439 the TMs, similar to the “open” conformation of CD81. **(Figure 4A, 4B)**.
440
441
442

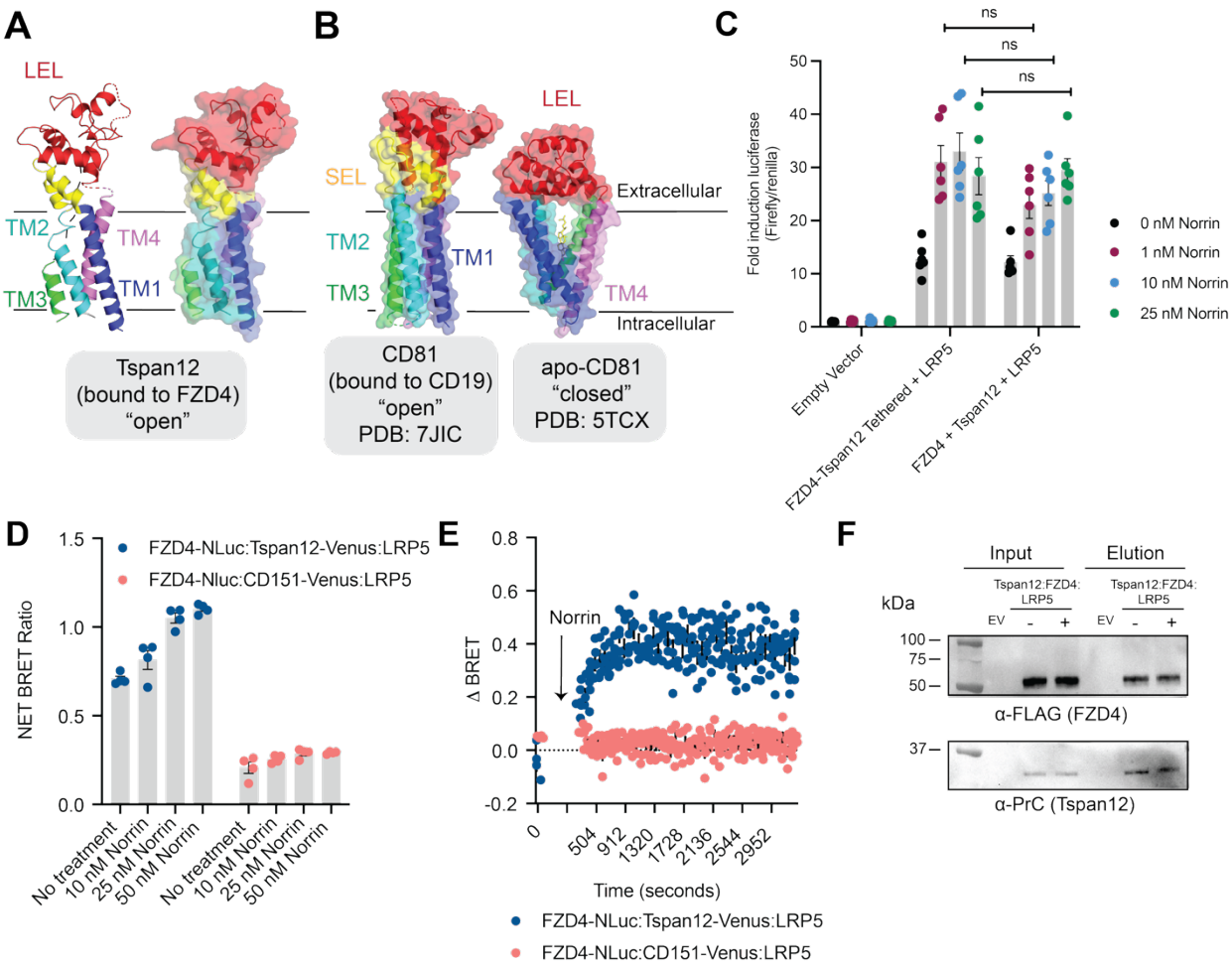

Figure 4: Tspan12 remains as a core component of the FZD4 signaling complex after Norrin recognition. (A) Structure of Tspan12 (bound to FZD4), highlighting an "open" state of Tspan12, with a closely packed four helix bundle orientation of the transmembrane helices. Tspan12 is colored by domain. **(B)** Comparison of "closed" apo-CD81 (right, PDB: 5TCX) with "open" CD19-complexed CD81 (left, PDB: 7JIC). The structures are colored by domain. The "open" conformation refers to an opening of the LEL away from the membrane. **(C)** TOPFlash signaling assay with tethered FZD4-Tspan12 or co-transfected FZD4 and Tspan12. Error bars represent mean ± SEM of two independent experiments, with three technical replicates each. Statistical analysis was performed in GraphPad Prism using an unpaired t-test, comparing tethered and co-transfected FZD4 and Tspan12 at each corresponding Norrin concentration. *p ≤ 0.05, **p ≤0.01, ***p ≤0.001, ns: not significant. Expression levels of FZD4 and Tspan12 constructs and co-transfection signaling controls are shown in Supplementary Figure 6. **(D)** BRET assay tracking Tspan12-FZD4 proximity. Fixed amounts of LRP5 and FZD4-NLuc were transfected into ΔFZD_{1-10} knockout cells with either CD151-Venus or Tspan12-Venus to assess the change in Tspan12-FZD4 proximity after 5 minutes of treatment with either 10 nM, 25 nM, or 50 nM Norrin. **(E)** Kinetic monitoring of Tspan12-FZD4 proximity upon 10 nM Norrin treatment in ΔFZD_{1-10} knockout cells expressing LRP5 and FZD4-NLuc with either Tspan12-Venus or the negative control, CD151-Venus. For BRET experiments in Panels D and E, data are presented as mean ± SEM of five technical replicates **(F)** Pulldown of PrC tagged Tspan12 associated with FLAG tagged FZD4 in untreated cells (-) or after 10 nM Norrin treatment (+) for 15 minutes in ΔFZD_{1-10} knockout cells co-transfected with PrC-Tspan12, FLAG-FZD4, and untagged LRP5. EV: empty vector

465 transfected cells. The blot in panel F represents one biological replicate that is representative of
466 two biological replicates.
467

468 To investigate whether Tspan12 dissociation from FZD4 is required for signaling, we
469 utilized our tethered FZD4-Tspan12 construct to determine if forcing the association of Tspan12
470 with FZD4 via covalent tethering inhibits signaling. If Tspan12 dissociation from FZD4, allowing
471 for LRP5/6 engagement, is a key step in the signaling mechanism, we would expect that the
472 forced recruitment of Tspan12 to FZD4 via tethering would result in decreased signaling, thereby
473 preventing LRP5/6 engagement and downstream signaling. Using the TOPFlash β-catenin
474 reporter assay in ΔFZD_{1-10} cells, we compared the ability of the tethered construct or co-
475 transfected FZD4 and Tspan12 to induce signaling under conditions with matched receptor levels
476 (**Figure 4C, Supplementary Figure 6B**). Tethered Tspan12-FZD4 signaled at levels matching
477 those of co-transfected FZD4 and Tspan12, indicating that dissociation of Tspan12 from FZD4 is
478 not strictly required for signaling.

479 In a series of orthogonal assays, we used a bioluminescence resonance energy transfer
480 (BRET) assay to monitor the association of Tspan12 with FZD4 in cells. We fused the luciferase
481 energy donor NanoLuc (NLuc) to FZD4 and energy acceptor Venus to Tspan12, or a negative
482 control, non-interacting tetraspanin, CD151, using previously reported linkers and insertion sites
483 **(Supplementary Table 2)** (59, 60). When in close proximity (within 10 nm (61)), NLuc and Venus
484 undergo BRET, generating a fluorescent signal. We used this system to determine if the amount
485 of Tspan12 in proximity to FZD4 changes after Norrin recognition. In cells co-transfected with
486 LRP5 and the BRET constructs, we either left the cells untreated or treated them with 10, 25, or
487 50 nM Norrin, and then measured the BRET ratio 5 minutes after Norrin addition **(Figure 4D)**.
488 Importantly, Tspan12-Venus and FZD4-NLuc showed a 4- to 5-fold increase in the BRET ratio
489 compared to our negative control, CD151-Venus, highlighting the assay's ability to detect the true
490 interaction between FZD4 and Tspan12 **(Figure 4D)**. If Tspan12 is dissociating from FZD4 after
491 Norrin treatment, we would expect to see a decrease in the BRET ratio, indicating decreased

492 proximity. However, the BRET ratio was slightly increased following Norrin treatment, again
493 suggesting that Tspan12 is not dissociating from FZD4 **(Figure 4D)**. To assess if Tspan12-FZD4
494 proximity changes over the time course of signaling, we transfected ΔFZD_{1-10} cells with our BRET
495 constructs and LRP5, collected a baseline reading, left the cells untreated or added 10 nM Norrin,
496 and then collected a time course of the BRET signal over a period of approximately 55 minutes
497 **(Figure 4E)**. Again, we observed that the BRET ratio was slightly increased and remained
498 constant throughout our entire data collection period, further suggesting that Tspan12 remains a
499 core component of the FZD4 complex after ligand recognition. Moreover, co-immunoprecipitation
500 of Tspan12 and FZD4 in cells with or without Norrin treatment showed similar amounts of Tspan12
501 pulled down in both conditions, providing additional evidence that Tspan12 remains associated
502 with FZD4 **(Figure 4F)**. Flow cytometry confirmed that most of the transfected receptor was found
503 on the cell surface rather than in the endoplasmic reticulum, confirming that our pulldown result
504 wasn't confounded by a large pool of intracellular receptor that is insensitive to Norrin binding
505 **(Supplementary Figure 9).** We saw no evidence for Tspan12 dissociation in three orthogonal
506 signaling assays. Indeed, the affinity of Norrin for Tspan12-FZD4 (low nM) is much higher than
507 the measured affinities of Norrin for LRP6 (~0.4-2.8 μM) (13, 62), suggesting that the efficiency
508 of this proposed competitive hand-off would be very low in cells. Instead, our data indicate that
509 Tspan12 remains a component of the Norrin signaling complex, which is also consistent with a
510 prior report that Tspan12 co-localizes with the FZD4-LRP5 signaling complex after Norrin binding
511 at the cell surface and in endosomes (63).
512
513 **DISCUSSION**
514
515 Here, we report the structure of the co-receptor Tspan12 bound to FZD4, showing that
516 Tspan12 and FZD4 form a direct complex in the absence of Norrin. Tspan12 engagement of
517 FZD4 enables higher affinity binding to Norrin, and our cell-based assays indicate that Tspan12
518 remains a core component of the FZD4-LRP5/6 signaling complex after Norrin recognition. This

raises a fundamental question: if Tspan12 is not dissociating from FZD4, how is LRP5/6 able to be recruited to the complex? One potential mechanism is that Tspan12 remains incorporated in the Norrin-FZD4-LRP5/6 complex, with Tspan12 and LRP5/6 each binding to opposite protomers of Norrin. Although Norrin is a disulfide-linked homodimer that is overall two-fold symmetric, the cysteine knot fold of Norrin results in distinct spatial orientations of each protomer, breaking perfect symmetry **(Figure 5A).** In the second Norrin protomer, the Tspan12 binding site is rotated approximately 90° **(Figure 5B).** The AlphaFold-Multimer model of Norrin bound to two Tspan12 molecules shows that this orientation results in the second Tspan12 molecule being rotated 90° perpendicular to the membrane plane, which would be physiologically incompatible with binding (**Supplementary Figure 10)**. This suggests a possible model in which Tspan12 binds to one protomer of Norrin and LRP5/6 binds to the opposite protomer of Norrin, leading to the formation of a stable Tspan12-FZD4-LRP5/6 signaling complex **(Figure 5C)**. Alternatively, it is also possible that the binding sites of Tspan12 and LRP5/6 are only partially overlapping, allowing LRP5/6 to engage both protomers of Norrin. The mechanism by which LRP5/6 integrates into the complex and the overall stoichiometry of the active signaling complex remain important open questions.

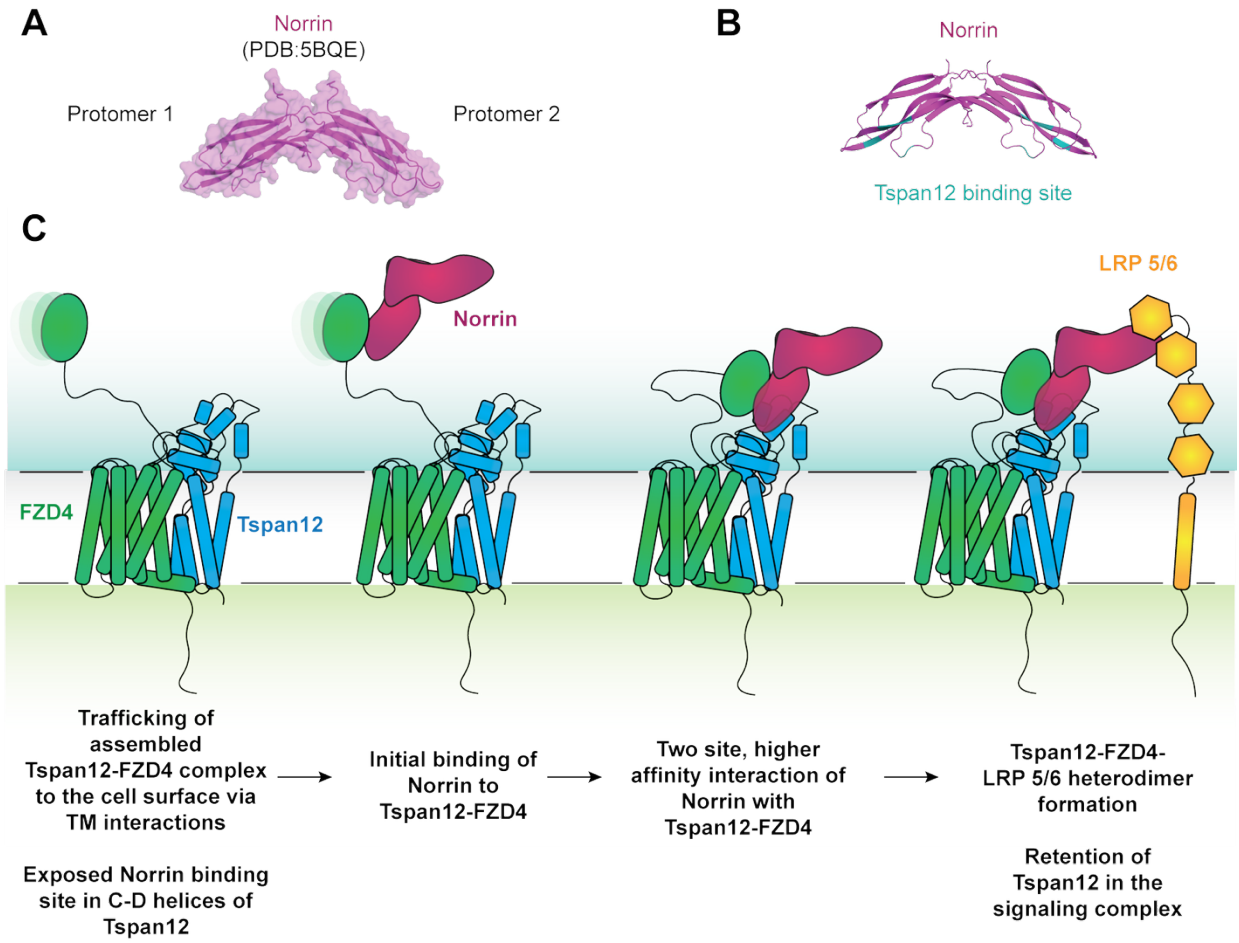

Figure 5: Proposed model for Tspan12 assembly into the Norrin-FZD4-LRP5/6 signaling complex. (A) Crystal structure of Norrin (PDB:5BQE). **(B)** Tspan12 binding site(37) mapped onto the surface of Norrin, highlighting distinct spatial orientations of the Tspan12 binding site on each protomer. Residues within 5 Å of Tspan12 in the Tspan12-Norrin AlphaFold3 model are colored in teal. **(C)** Proposed model for incorporation of Tspan12 into the Norrin-FZD4-LRP5/6 signaling complex. Tspan12 is trafficked to the cell surface in conjunction with FZD4 and exists in a complex with FZD4 prior to Norrin recognition. Norrin engages in a two-site interaction with Tspan12-FZD4 to recruit LRP5/6 into a Tspan12-FZD4-LRP5/6-Norrin signaling complex. Although this model depicts LRP5/6 interacting with only one Norrin promoter for simplicity, the mechanism by which LRP5/6 engages Norrin and incorporates into the complex remains an open question.

Wnts contact FZDs through a highly conserved two-site mechanism, positioning “thumb” and “finger” domains on opposite sides of the CRD (5). Why Wnts need a two-site mode of engagement is debated, but one model is that it provides specificity, avidity, and optimally orients the Wnt ligand for LRP5/6 engagement (5, 64). Importantly, Norrin contacts the CRD of FZD4 at

564 a single site (65, 66), suggesting that a function of Tspan12 may provide to additional binding site
565 to facilitate LRP5/6 recruitment and downstream signaling. The C-D helices of Tspan12 are
566 anchored close to the membrane in our structure. Our results suggest that one role of Tspan12
567 may be to prevent Norrin from diffusing away by providing avidity through its additional binding
568 site and to restrain the motion of Norrin bound to the highly dynamic CRD-Hinge region of FZD4,
569 facilitating proper orientation of Norrin to increase the likelihood of LRP5/6 recruitment. Structural
570 characterization of the native FZD4-Tspan12-LRP5/6-Norrin complex and Wnts in complex with
571 full-length FZD receptors and LRP5/6 will be necessary to answer this question and will remain
572 an important area of future investigation.

573 The partnership between FZD4 and Tspan12 represents an important, heretofore
574 unappreciated function of tetraspanins in the direct regulation of receptor signaling. Tetraspanins
575 are recognized as “molecular facilitators” (21), acting as chaperones to traffic partner proteins to
576 the cell surface and regulate their plasma membrane localization (22, 53). However, they are not
577 appreciated as a family of membrane proteins that directly signal or bind to endogenous ligands.
578 The finding that Tspan12 directly binds to Norrin with high affinity (37) and our findings that
579 Tspan12 increases the affinity of Norrin binding, while remaining a component of the active Norrin-
580 FZD4-LRP5/6 signaling complex, highlight an important role for tetraspanins in the direct
581 regulation of signaling, rather than simply functioning as molecular chaperones in the membrane.
582 10 out of 33 human tetraspanins have an intracellular tail, indicating that more tetraspanins than
583 appreciated may play a direct role in signal transduction. The 59 amino acid C-terminal
584 cytoplasmic tail of Tspan12 contains several putative phosphorylation sites, suggesting it may
585 play a role in signaling by scaffolding the recruitment of intracellular signaling molecules. Early
586 work in the tetraspanin field showed that several tetraspanins could co-immunoprecipitate
587 phosphoinositide 4-kinase (67) and protein kinase C (PKC) (68), suggesting that tetraspanins
588 may recruit these kinases to specific membrane locations to influence signaling. More recent work
589 has elegantly shown that in B cells, the N-terminal intracellular domain of tetraspanin CD53

590 promotes the recruitment of protein kinase C family member PKCβ to CD53-containing
591 microdomains, thereby facilitating PKC-mediated phosphorylation of substrates (69). An
592 important area of future studies will be to characterize whether signaling molecules bind to the
593 intracellular tail of Tspan12 and play a role in amplifying β-catenin signaling, as well as to
594 determine whether any other tetraspanins directly bind an endogenous ligand within their
595 ectodomain.

596 Modulation of β-catenin signaling is an area of active therapeutic investigation for cancer,
597 degenerative diseases, and diseases related to blood vessel angiogenesis, like FEVR (1, 70).
598 Mutations in Tspan12 are found in approximately 5-10% of FEVR patients (18, 19, 29–33).
599 Mapping known missense mutations found in FEVR patients onto the structure of FZD4-Tspan12
600 revealed that these mutations do not map to the Tspan12-FZD4 binding interface
601 **(Supplementary Figure 11)**, suggesting instead that these mutations likely decrease Norrin
602 binding or affect protein quality or folding. Targeting the β-catenin pathway remains challenging
603 due to the toxicity associated with broad inhibition of β-catenin signaling. While FZD4 and LRP5/6
604 are widely expressed throughout the body, Tspan12 has more limited expression (35), offering a
605 potentially powerful way to specifically modulate Norrin signaling for the treatment of diseases of
606 retinal hypo-vascularization, such as FEVR, or for ocular diseases associated with retinal hyper-
607 vascularization, such as diabetic retinopathy. Tspan12 antibodies that inhibit Norrin signaling and
608 decrease angiogenesis have been reported (71). Our results suggest that because Tspan12
609 forms a direct complex with FZD4, modulates how FZD4 binds to Norrin, and stays engaged with
610 the LRP5/6 signaling complex, antibodies that either block the Norrin binding site on Tspan12 or
611 stabilize the interaction of Norrin with Tspan12 may offer new ways to treat diseases
612 characterized by retinal hyper-vascularization and hypo-vascularization, respectively.

613
614
615 **ACKNOWLEDGEMENTS**

616 This work was funded by an NIH grant DP5OD036136 and a UCSF Sandler Fellowship to K.J.S,
617 and an NIH IMSD training grant 5R25GM056847-25 and Achievement Rewards for College
618 Scientists (ARCS) scholarship to K.A.E.A. We thank members of the Susa and Manglik labs, Dr.
619 Elise Bruguera for helpful discussions, the Manglik lab for the use of equipment, and Dr. Meredith
620 Anne Skiba for the anti-F_{ab} nanobody. We thank Dr. Julia Maria Rogers, Dr. Edward Harvey, and
621 Dr. Aashish Manglik for feedback on the manuscript. Cryo-EM data were collected at the Cryo-
622 EM facility at the University of California, San Francisco. We thank Dr. Glenn Gilbert for helpful
623 comments and assistance during grid screening and data collection. We thank Benoit
624 Vanhollebeke for generating and generously sharing ΔFZD_{1-10} HEK293T cells (72).
625

626 **AUTHOR CONTRIBUTIONS**

627 K.J.S. designed and conceived of the project. A.J.G., P.P.P., K.A.E.A, and K.J.S. designed
628 experiments. A.J.G. and K.J.S. prepared the sample for cryo-EM, and A.J.G., K.J.S., and P.P.P.
629 collected and processed cryo-EM data. P.P.P. and K.J.S. performed model building and
630 refinement. A.J.G., P.P.P., K.A.E.A., and K.J.S. performed cell-based assays. K.J.S. wrote the
631 manuscript with input from all authors. K.J.S. supervised the work and provided financial funding.
632

633 **COMPETING INTERESTS STATEMENT**

634 The authors declare no competing interests.
635
636 **DATA AND MATERIALS AVAILABILITY**

637 Materials will be made available upon request. Protein Data Bank (PDB) and Electron
638 Microscopy Data Bank (EMDB) IDs of the FZD4-Tspan12-BRIL F_{ab} model and map are 9YEV
639 and EMD-72864, respectively.
640
641 **METHODS**

642 **Design of FZD4-Tspan12 fusion protein**

643 The FZD4-Tspan12 fusion was cloned into a doxycycline-inducible pcDNA3.1 (+) tet/zeo vector
644 with an N-terminal haemagglutinin signal sequence followed by a FLAG epitope tag. Residues
645 37-537 of human FZD4 (full length, excluding the endogenous signal sequence) were connected
646 to full-length human Tspan-12 (residues 2-305) using a GGGSx4 linker. The linker length was
647 engineered to be long enough in length to ensure tethering of Tspan12 would not enforce Tspan12
648 engagement on one side of FZD4. For the BRIL FZD4-Tspan12 construct, BRIL replaced ICL3
649 (residues 416-427) of FZD4 using linkers derived from the A_{2A} adenosine receptor (ARRQL
650 between residue 415 and the N-terminus of BRIL, and ARSTL between the C-terminus of BRIL
651 and residue 428). Tspan12 was linked to FZD4-BRIL with a GGGSx4GGSx3 linker. BRIL insertion
652 was guided by monitoring the rigidity of the BRIL linkage using AlphaFold3, and the insertion
653 linkage was modified using the strategy for a previously reported FZD5-BRIL fusion(40).
654
655 **Protein expression and purification of FZD4-BRIL-Tspan12 complexes**
656 The FZD4-Tspan12 fusion protein was expressed in Expi293F TetR cells containing a stably
657 integrated tetracycline repressor grown in Expi293 (Thermo) media supplemented with 20 µg/mL
658 Blasticidin (Invivogen). 500 mL of Expi293F TetR cells were grown to a density of approximately
659 2.8 x 10^6 cells/mL and then transiently transfected with 0.4 mg of DNA and 400 µL FectoPro
660 transfection reagent (Polyplus). 24 hours after transfection, the cells were fed 3 mM valproic acid
661 sodium salt (Sigma-Aldrich) and 4.5 mL of 45% D-(+)-Glucose solution (Sigma-Aldrich). 24 hours
662 later, the transfected cells were induced with 5 mL 0.4 mg/mL doxycycline hyclate. 24 hours after
663 induction, cells were harvested by centrifugation at 4000 x g for 10 minutes at 4°C. The mass of
664 the pellet was recorded, and then the pellet was flash frozen and stored at -80°C until use.
665
666 The complex was purified similarly to a previously described protocol (38). Cells were thawed and
667 then lysed by osmotic shock in 150 mL buffer containing 20 mM HEPES, pH 7.4, 2 mM
668 magnesium chloride, 2 mg/mL iodoacetamide (Sigma Aldrich), and 1:100,000 (v:v) benzonase

669 nuclease (Sigma Aldrich). Lysed cells were centrifuged at 18,000 × g for 20 minutes at 4°C. FZD4-
670 Tspan12 was then extracted from the pellet using a glass dounce in 150 mL solubilization buffer
671 containing 20 mM HEPES pH 7.4, 250 mM NaCl, 10% (v/v) glycerol, 1% (w/v) n-Dodecyl-β-D-
672 Maltoside (DDM - Anagrade; Anatrace), 0.1% (w/v) cholesterol hemisuccinate (CHS;Steraloids),
673 and 2 mg/mL iodoacetamide. The sample was stirred for 2 hours at 4°C and then centrifuged at
674 20,000 × g for 30 minutes at 4°C. The supernatant, supplemented with 2 mM calcium chloride,
675 was filtered through a glass microfiber prefilter and loaded by gravity flow onto 2.5 mL of M1 anti-
676 FLAG antibody affinity resin. The resin was washed with 100 mL of buffer containing 20 mM
677 HEPES pH 7.4, 150 mM NaCl, 2 mM $CaCl_2$, 0.1% DDM, and 0.01% CHS, and then 100 mL of
678 buffer containing 2 mM $CaCl_2$, 150 mM NaCl, 20 mM HEPES pH 7.4, 0.05% GDN (Anatrace),
679 and 0.005% CHS. Bound protein was eluted in 20 mL buffer containing 20 mM HEPES pH 7.4,
680 150 mM NaCl, 0.05% GDN, and 0.005% CHS, 5 mM EDTA, and 0.2 mg/mL FLAG peptide. The
681 eluate was concentrated in a 100 kDa MWCO centrifugal filter and then complexed with anti-BRIL
682 Fab and anti-Fab nanobodies (Nb). FZD4-Tspan12 was incubated with anti-BRIL Fab and anti-
683 Fab Nb at a 1:1.4:2 molar ratio, respectively, on ice for 1 hour. The complex was then purified by
684 size exclusion chromatography (SEC) on a Superose 6 column (GE Healthcare) in buffer
685 containing 20 mM HEPES pH 7.4, 150 mM NaCl, 0.05% GDN, and 0.005% CHS. Immediately
686 after the FZD4-Tspan12-Fab-Nb complex eluted from the S6 column, two fractions were
687 concentrated to 3.65 mg/mL using a 100k MWCO centrifugal filter and then applied to grids. Purity
688 and monodispersity of the sample for cryo-EM were evaluated by SDS-PAGE and SEC
689 **(Supplementary Figure 1)**.
690

691 **Purification for anti-BRIL Fab**

692 The heavy and light sequences of the previously described anti-BRIL Fab (BAG2) (43) were
693 cloned into the pTarget and p261040 (Atum) vectors, respectively. A set of previously described
694 stabilizing mutations (SSASTKG replaced with FNQIKG) were introduced into the hinge region of

695 the heavy chain to increase its rigidity (73). The Fab was expressed similarly to a previously
696 described protocol (56). 500 mL of Expi293F cells at a density of 2.8 x 10^6 cells/mL were
697 transfected with 0.2 mg heavy chain DNA, 0.2 mg light chain DNA, and 200 µL FectoPro
698 transfection reagent (Polyplus). Approximately 20 hours after transfection, cells were fed with 3
699 mM valproic acid sodium salt (Sigma-Aldrich) and 4.5 mL of 45% D-(+)-Glucose solution (Sigma-
700 Aldrich) and then cultured for 5 days. The culture was harvested by centrifugation at 4000 × g for
701 15 minutes at 4°C. The supernatant was loaded onto 2.5 mL CaptureSelect CH1-XL Affinity Matrix
702 resin (ThermoScientific Cat. No.1943462005). The resin was washed with 100 mL buffer
703 containing 20 mM HEPES, pH 7.4, and 150 mM NaCl, and protein was eluted in 15 mL 100 mM
704 citrate buffer, pH 3.0. The eluted protein was neutralized with buffer containing 1 M HEPES, pH
705 8. Protein was then concentrated using an Amicon 30 kDa MWCO centrifugal filter to a final
706 volume of approximately 2 mL (17 mg/mL) and dialyzed overnight into phosphate-buffered saline
707 (PBS). Protein purity was analyzed using an SDS-PAGE Coomassie-stained gel, and protein
708 aliquots were flash-frozen in liquid nitrogen and stored at -80 °C. Before complexing to FZD4-
709 Tspan12, anti-BRIL Fab and anti-Fab nanobody were buffer-exchanged into buffer containing 20
710 mM HEPES pH 7.4, 150 mM NaCl, 0.05% GDN, and 0.005% CHS (w/v).
711
712 **Cryo-EM sample preparation and data collection**
713 Samples for cryo-EM were prepared on Quantifoil holey carbon film-coated 400 mesh gold grids
714 (Electron Microscopy Sciences, R1.2/1.3, Cat: N1-C14nAu40-01). Grids were glow-discharged
715 before the application of 3.5 µL of the sample (3.6 mg/mL). After blotting for 5.5 s with a blot force
716 of 5, the grids were plunge-frozen in liquid ethane using a FEI Vitrobot Mark IV (FEI) with 100%
717 chamber humidity at room temperature.
718
719 **Cryo-EM data processing and model building**

720 Grids were loaded onto a 2nd-generation Titan Krios, and data collection was automated through
721 Serial EM(74). Collection parameters are shown in Supplementary Table 1. Micrographs were
722 imported into CryoSPARC v4.5.3(75) and processed as shown in Supplementary Figure 2A to
723 resolve the FZD4-BRIL-Tspan12 fusion construct in complex with BRIL fab and anti-fab nanobody
724 to 3.38 Å (best overall map) and 3.55 Å (Tspan12 focused map) using non-uniform refinement
725 (76). The Tspan12-focused map was further processed to 3.4 Å using Deep EMhancer (77, 78).
726
727 Model building was carried out using both non-uniform refinement and deepEMhancer maps
728 overlayed in Coot(79). The AlphaFold3 models of Tspan12 and FZD4-BRIL and the atomic
729 coordinates of the BRIL Fab and anti-Fab nanobody (PDB: 6WW2 were manually fitted into the
730 density map using ChimeraX to generate a starting model(80). The transmembrane domains and
731 extracellular domains of Tspan12 docked into the density separately to allow for fitting. The
732 coordinates were then manually rebuilt using Coot(79). TM4 of Tspan12 was poorly resolved and
733 modeled as polyalanine, and side chains with poor density within the Tspan12 LEL or TMs with
734 poor density were truncated to Cβ. All models were refined in Phenix RealSpace Refine (81, 82)
735 with secondary structure restraints against the 3.4. map from non-uniform refinement in
736 cryoSPARC. The final models were evaluated by MolProbity and EMRinger (83, 84). Statistics of
737 the map reconstruction and model refinement are presented in Supplementary Table 1. Structural
738 biology applications used in this project (other than CryoSPARC) were compiled and configured
739 by SBGrid (85). Structural depictions were created through UCSF ChimeraX.
740
741 **Tspan12 trafficking assay**
742 2 mL of Expi293F TetR cells were seeded at 2.8E6 cells/mL in a 6 well plate and then transfected
743 using FectoPro (PolyPlus) with either: **1)** 1.5 ug empty pcDNA3.1tet/zeo (+) vector, **2)** 0.75 ug
744 empty pcDNA3.1tet/zeo (+) vector and 0.75 ug pcDNA3.1tet/zeo (+) Tspan12, **3)** 0.75 ug
745 pcDNA3.1tet/zeo (+) FLAG-FZD4 (full-length, WT or a chimeric construct) and 0.75 ug

746 pcDNA3.1tet/zeo (+) Tspan12 (full-length), or **4)** 1.5 ug FLAG-FZD4-Tspan12 fusion. 24 hours
747 after transfection, 3 mM valproic acid sodium salt (Sigma-Aldrich) and 18 µL of 45% D-(+)-
748 Glucose solution (Sigma-Aldrich) were added to the cultures. 24 hours later, receptor expression
749 was induced with 20 µL of 0.4 mg/mL doxycycline hyclate. 24 hours after induction, cells were
750 harvested by centrifugation at 4000 x g for 10 minutes at 4°C. Approximately 500,000 cells were
751 added to each well of a V-bottom 96-well plate (Costar), and cells were washed with cold PBS.
752 Cells were then incubated on ice for 30 minutes with 10 µg/mL Alexa 488-anti-M1 FLAG
753 (hybridoma) and Alexa 647-anti-Tspan12 (Biotechne Catalog #: FAB8910R) in 20 mM HEPES
754 buffer pH 7.4, containing 150 mM NaCl, 2 mM CaCl2, and 0.1% BSA. Cells were washed twice
755 with cold PBS and analyzed on an Agilent Novocyte 3000.
756 For western blots assessing the total cell levels of Tspan12, transfected cells were harvested by
757 centrifugation at 4000 x g for 10 minutes at 4°C. The supernatant was discarded, and the cell
758 pellet was lysed in 1 mL SDS loading dye supplemented with benzonase. 10 µL of lysate was run
759 on a non-reducing SDS-PAGE gel, and the protein was transferred to a nitrocellulose membrane.
760 The transferred protein was visualized with Ponceau staining, and then the membrane was
761 blocked at room temperature for 1 hour in TBST (0.1% Tween-20 in Tris-buffered-saline) with 5%
762 (w/v) Bovine Serum Albumin (BSA) (Fisher Scientific BP9706100). The blocked membrane was
763 cut and then incubated overnight at 4°C with shaking in TBST with 1% (w/v) BSA containing either
764 FLAG-HRP conjugate antibody (Cell Signaling 86861S**;** 1:1,000 dilution) or anti-Protein C (PrC)
765 tag antibody (homemade from murine HPC4 hybridoma, 1:5000 dilution of 0.5 mg/mL stock)
766 supplemented with 2 mM $CaCl_2$. The next morning, the Tspan12-PrC blot was incubated with anti-
767 mouse IgG HRP Conjugate (Cell Signaling 7076S; 1:5,000) in TBST with 1% (w/v) BSA for 1 hour
768 at room temperature with shaking. Blots were washed with 10 mL of TBST three times, each for
769 5 minutes. Blots were developed with Western Lightning Plus-ECL, Enhanced
770 Chemiluminescence Detection Kit (PerkinElmer), and then imaged.
771

772 **Expression and purification of MBP-Norrin**

773 MBP-Norrin was expressed and purified as previously described (37, 59). MBP-3C-Norrin (33-
774 133)-1D4 with an IL2 signal sequence was cloned into the pFUSE vector (Invitrogen). 500 mL of
775 Expi293 cells were grown to a density of approximately 2.8 x 10^6 cells/mL and then transiently
776 transfected with 0.4 mg of DNA and FectoPro transfection reagent (Polyplus) at a 1:1
777 DNA/FectoPro ratio. 24 hours after transfection, the cells were fed 3 mM Valproic acid sodium
778 salt (Sigma-Aldrich) and 4.5 mL of 45% D-(+)-Glucose solution (Sigma-Aldrich). 9 days after
779 transfection, the culture was harvested by centrifugation at 4000x g for 15 minutes at 4°C. The
780 culture supernatant was loaded onto 2 mL amylose resin (New England Biolabs). The resin was
781 washed with 5 column volumes of buffer containing 20 mM HEPES pH 8, 150 mM NaCl, 1 mM
782 EDTA, and 5% glycerol. Bound protein was eluted in 20 mL of buffer containing 20 mM HEPES
783 pH 8, 150 mM NaCl, 1 mM EDTA, 5% glycerol, and 10 mM maltose. Eluted MBP-Norrin was
784 concentrated using a 30 MWCO spin concentrator (Amicon), and concentrated protein was
785 loaded on a Superdex 200 Increase 10/300 GL equilibrated in buffer containing 20 mM HEPES
786 pH 8, 150 mM NaCl, 1 mM EDTA, and 5% glycerol. Peak fractions were pooled, concentrated to
787 approximately 1 mg/mL, flash frozen, and frozen in 25 µL aliquots at -80°C until use
788 **(Supplementary Figure 12)**. MBP-Norrin was validated in FZD4 binding assays before use.

789

790 **MBP-Norrin binding assays**

791 2 mL of Expi293F TetR cells were seeded at 2.8E^6 cells/mL in a 6 well plate and then transfected
792 using FectoPro (PolyPlus) with either 1.5 µg empty pcDNA3.1tet/zeo (+) or 1.5 ug of FLAG-apo-
793 FZD4, FLAG-FZD4-BRIL-Tspan12, E170K FLAG-FZD4-BRIL-Tspan12, or FLAG-FZD4 with the
794 CRD and hinge of FZD10. 24 hours after transfection, cells were fed with 3 mM valproic acid
795 sodium salt (Sigma-Aldrich) and 18 µL of 45% D-(+)-Glucose solution (Sigma-Aldrich). 24 hours
796 later, expression was induced with 20 µL of 0.4 mg/mL doxycycline hyclate (dissolved in buffer
797 containing 20 mM HEPES pH 7.4, 150 mM NaCl). 24 hours later, cells were harvested by

798 centrifugation at 4,000 x g at 4 °C and resuspended in cold phosphate buffered saline (PBS). The
799 cells were then counted, and 100,000 cells were added to each well of a V-bottom 96-well plate
800 (Grenier Bio). Cells were washed again with 100 µL cold PBS and then incubated with different
801 concentrations of either the 1D4-tagged MBP-Norrin, secondary antibody alone (anti-1D4-488),
802 M2-FLAG-488 to quantify receptor expression level, or buffer alone for thirty minutes at 4°C.
803 Following another PBS wash, cells were incubated with 2 µg/mL anti-Rho1D4-Alexa Fluor 488
804 antibody for 30 minutes at 4°C to detect Norrin binding. After secondary antibody incubation, cells
805 were washed twice more with PBS and were analyzed by flow cytometry using a Novocyte 3000
806 (Agilent). Live/dead gates were set using SSC-A versus FSC-A and singlet gates using FSC-H
807 versus FSC-A, and fluorescence intensity in the 488 channel was recorded in the doubly gated
808 population. Median fluorescence intensity (MFI) at 488 nm was plotted in GraphPad Prism as an
809 assessment of MBP-Norrin binding to cells. For EC50 calculations, non-specific signal was
810 subtracted (MFI in the mock condition treated with the corresponding MBP-Norrin concentration).
811 Curve fitting was performed in Prism (GraphPad, v10) to a log (agonist) vs. response four-
812 parameter model, with no constraints on Hill Slope, EC50, or top values, and a constraint of 0 on
813 the bottom value.
814
815 **BRET assays**
816 ΔFZD_{1-10} HEK293T cells were used for all BRET experiments. White 96-well tissue-culture
817 treated plates (Revity) were precoated with 50 µL/well of a 0.1 mg/mL poly-D-lysine (Sigma) and
818 incubated at room temperature for 20 minutes. The coating solution was aspirated and washed
819 once with 200 µL/well of DPBS, and the plate was dried for 20 minutes in the tissue culture hood
820 before seeding cells. ΔFZD_{1-10} HEK293T cells were trypsinized and diluted to $0.4E^5$ cells/mL. 1
821 mL of cells at $0.4E^6$/mL were then transfected in suspension. Acceptor: donor transfection ratios
822 were pre-determined from acceptor: donor titration experiments to determine the signal plateau
823 and fold increase over the CD151-Venus negative control. For transfections, Tube A contained

824 40 µL opti-MEM, 20 ng FZD4-NLuc, 100 ng Tspan12-Venus or CD151 Venus, or 0 ng of a Venus
825 construct as a background control, and 20 ng untagged LRP5. An empty pcDNA3.1 vector was
826 used to bring the final DNA concentration to 1,000 ng. Tube B contained 49 µL Opti-MEM and 1
827 µL Lipofectamine 2000. Tubes A and B were incubated separately for 5 minutes and then added
828 together and incubated at room temperature for 10 minutes. The transfection mix was added
829 dropwise to 1 mL of cells at $0.4E^6$/mL, 100 µL of the cell-transfection mix was added to each well
830 of the poly-D-lysine-coated 96-well plate. Approximately 24 hours after transfection, the cells were
831 washed once with 200 µL of HBSS and then kept in HBSS. 10 µL of furimazine (Promega) (final
832 dilution at 1:1000) was added to a final volume of 90 µL, and 5 min after furimazine addition,
833 luminescence was read three times for a baseline reading. Subsequently, 10 µL of Norrin at a
834 final concentration of 10 nM (in HBSS) was added to a final volume of 100 µL, and luminescence
835 reading was continued 44 times for a total of 54.8 minutes. All measurements were performed at
836 37°C using a ClarioStar plate reader. BRET experiments were performed with five replicates.
837
838 **Tspan12 Pulldown**
839 ΔFZD_{1-10} HEK293T cells were seeded at $0.3E^6$ cells/mL in 10 mL DMEM with 10% FBS (Fisher
840 Scientific SH3007003HI) and 1% Pen-Strep (Thermo Scientific 15140122). Approximately 12
841 hours later, media was replaced with 10 mL DMEM with 2% FBS and no Pen/Strep. Per 10 cm^3
842 plate, cells were transfected with 1.2 ug DNA, at a ratio of 1:1.5:4 FZD4:LRP5:Tspan12, or 1.2
843 µg empty vector (pcDNA3.1), and 40 µL lipofectamine 2000 in 1.5 mL opti-MEM. The FZD4
844 construct was N-terminally FLAG tagged, Tspan12 was N-terminally Protein C (PrC) tagged, and
845 LRP5 was untagged. The transfection mix was incubated for 15 minutes at room temperature and
846 then added dropwise to the cells. The next day, the media was replaced with DMEM with 10%
847 FBS and 1% Pen-Strep. 48 hours after transfection, cells were serum starved for 1 hour in DMEM
848 with no FBS and then treated with 10 nM of Norrin for 15 minutes or left untreated. Cells were
849 harvested in 2 mL cold PBS with 5 mM EDTA, pelleted at 4000 x g for 10 minutes at 4°C.

850 Pulldowns were performed as previously described (56). Briefly, the pellet was lysed by osmotic
851 shock in buffer containing 20 mM HEPES pH 7.4, 2 mM $MgCl_2$, 2 mg/mL iodoacetamide, and
852 1:100,000 v:v benzonase. Samples were rotated for 30 minutes at 4°C and then centrifuged at
853 16,000 × g for 15 minutes at 4°C. Solubilization buffer (1% (w/v) DDM/0.1% CHS buffer, 20 mM
854 HEPES pH 7.4, 250 mM NaCl, 10% glycerol, 2 mg/mL iodoacetamide) was added to the pellet,
855 and then the samples were rotated for 2 hours at 4°C. Samples were pelleted at 20,000 x g for
856 30 minutes at 4°C and then added to 25 µL of M2 magnetic FLAG beads (Sigma, M8823). The
857 samples were rotated for 2 hours in the cold room, and then beads were washed three times with
858 1 mL of buffer containing 0.1% (w/v) DDM, 0.01% CHS buffer, 20 mM HEPES pH 7.4, 150 mM
859 NaCl. Proteins bound to the beads were eluted in 250 µL SDS loading dye supplemented with
860 0.2 mg/mL FLAG peptide.
861
862 Western blot analysis was performed similarly to a previously described protocol (56). 10% input
863 and 10% eluate samples were run on a non-reducing SDS-PAGE gel, and then the protein was
864 transferred to a nitrocellulose membrane. Next, the membrane was blocked in TBST with 5%
865 (w/v) BSA (Fisher Scientific BP9706100) at room temperature for 1 hour, shaking. The membrane
866 was then cut and incubated in TBST with 1% (w/v) BSA containing either FLAG-HRP conjugate
867 antibody (Cell Signaling 86861S**;** 1:1,000 dilution) or anti-Protein C (PrC) tag antibody (Cell
868 Signaling 68083; 1:1000 dilution), overnight at 4°C with shaking. The next morning, the Tspan12-
869 PrC blot was incubated with anti-Rabbit IgG HRP Conjugate (Cell Signaling 7074S; 1:5,000) in
870 TBST with 1% (w/v) BSA for 1 hour at room temperature with shaking. Blots were washed three
871 times with 10 mL of TBST and then developed with Western Lightning Plus-ECL, Enhanced
872 Chemiluminescence Detection Kit (PerkinElmer) prior to imaging.
873
874 **TOPFlash Signaling Assays**

875 ΔFZD1–10 HEK293T were used for all TOPFlash assays. White 96-well tissue-culture treated
876 plates (Revity) were precoated with 80 µL/well of a 0.1 mg/mL poly-D-lysine solution (Sigma) and
877 incubated at room temperature for 20 minutes. The coating solution was aspirated and washed
878 once with 100 µL/well of DPBS. The plate was then dried for 20 minutes in the tissue culture hood
879 before seeding the cells. For tethered FLAG-FZD4-Tspan12 versus FLAG-FZD4 and Tspan12
880 co-transfections (Figure 4C), Tube A contained 250 uL of OptiMEM, 250 ng of Super 8x TOPFlash
881 plasmid M50 (Addgene #12456), 50 ng Renilla luciferase control plasmid (pRL-TK, Promega),
882 250 ng of LRP5, 10 µg of FLAG-FZD4-Tspan12 or co-transfections of 200 ng FLAG-FZD4 with
883 600 ng Tspan12. For all other constructs tested, Tube A contained 250 uL of OptiMEM, 250 ng
884 of Super 8x TOPFlash plasmid M50 (Addgene #12456), 50 ng Renilla luciferase control plasmid
885 (pRL-TK, Promega), 50 ng of LRP5, 50 ng FLAG-FZD4 with 250 ng Tspan12. Empty pcDNA3.1
886 vector was used to bring to a final concentration of DNA to 2,500 ng for Tspan12 and FZD4 co-
887 transfections. Empty pcDNA3.1 vector was used as a control and included Super 8x TOPFLASH
888 plasmid M50 and Renilla luciferase control plasmid (pRL-TK). Tube B contained 250 µL of
889 OptiMEM with Lipofectamine 2000 (2 µL per 1 µg of DNA). Tubes A and B were incubated
890 separately for 5 minutes and then combined to incubated for 15-30 minutes. ΔFZD1–10 HEK293T
891 cells were trypsinized and diluted to $0.5E^6$ cells/mL with DMEM (10% FBS, 1% PenStrep). 2.5 mL
892 of cells at $0.5E^6$/mL were then added to the combined Tube A+B incubation. 100 µL of transfected
893 cells were added to the poly-D-lysine coated plates (12 wells per construct) and 1.2 mL of
894 transfected cells were plated in 12-well plates for companion flow staining assay (described
895 below). 24 hours post-transfection, media was aspirated and replaced with DMEM (0% FBS, no
896 PenStrep) with 10 nM C59-porcupine inhibitor (VWR) that contained either 0 nM MBP-Norrin
897 (control), 1 nM MBP-Norrin, 10 nM MBP-Norrin, or 25 nM MBP-Norrin, in triplicate. For the
898 companion flow assay to detect receptor expression levels, the media was swapped with DMEM
899 (0% FBS, no PenStrep) with 10 nM C59-porcupine inhibitor without Norrin. 24 hours after media
900 swap, media was aspirated and cells were washed with 100 µL DPBS (Corning). The Dual

901 Luciferase Assay Kit (Promega, #E1910) was used for TopFlash readout. Cells were lysed with
902 20 µL of 1x Passive Lysis Buffer for 20 minutes while shaking at room temperature. A ClarioStar
903 plate reader with dual injector was used to inject 20 µL of LARII reagent into each well and firefly
904 luciferase bioluminescence was recorded (580 ± 80 nm range and 10 second interval time). This
905 was immediately followed by injection of 20 µL of 1x Stop-and-Glo reagent per well and Renilla
906 luciferase bioluminescence was recorded (480 ± 80 nm range and 10 second interval time).
907
908 For FZD4/Tspan12 constructs used in the TOPFlash assay, expression levels were monitored
909 using flow cytometry. 36-48 hours after transfection (described above), and 18-24 hours after
910 DMEM (0% FBS, no PenStrep) media swap, the media was aspirated from the 12-well plates,
911 and 1.0 mL of cold PBS + 3 mM EDTA was added to the wells and mixed well to suspend the
912 cells. 200 µL of cells were added to 4 wells in 96-well v-bottom clear flow plates, kept on ice. Cells
913 were spun down at 300 g for 3 minutes and then washed with 100 µL of cold PBS, followed by a
914 second spin down. Cells were then suspended and double-stained with anti-FLAG M2 antibody
915 conjugated to Alexa Fluor 488 (final concentration, 1 µg/µL) and anti-Tspan12 antibody
916 conjugated to Alexa Fluor 647 (final concentration, 1 µg/µL) in HBS + 0.2% BSA for 30 minutes
917 on ice, protected from light. Unstained control samples were kept in HBS + 0.2% BSA and no
918 antibodies were included. After incubation, cells were washed spun down and washed 2x with
919 cold PBS before final suspension in cold PBS+3mM EDTA+1% BSA. Fluorescence was analyzed
920 on an Agilent Novocyte 3000.
921 **Flow Cytometry on Fixed and Permeabilized Cells**
922 ΔFZD1–10 HEK293T cells were seeded at 0.3E6 cells/mL in 2 mL DMEM with 10% FBS (Fisher
923 Scientific SH3007003HI) and 1% Pen-Strep (Thermo Scientific 15140122) in 6-well plates
924 (CytoOne). Approximately 12 hours later, media was replaced with 2 mL DMEM with 2% FBS and
925 no Pen/Strep. Cells were transfected with 0.3 µg DNA, at a ratio of 1:1.5:4 FZD4:LRP5:Tspan12,
926 or 0.3 µg empty vector (EV) (pcDNA3.1), and 10 µL lipofectamine 2000 in 500 µL opti-MEM. 12

927 hours after transfection, media was replaced with 2 mL DMEM with 10% FBS. 48 hours after
928 transfection, cells were harvested with 1 mL cold PBS +5 mM EDTA and placed in 1.5 mL
929 Eppendorf tubes. Cells were spun down at 300g, for 3 min (4°C) to pellet the cells. Media was
930 aspirated, and the cell pellet was resuspended in 1.3 mL of cold PBS. Cells were then divided
931 into two 96-well V-bottom plates (Costar) – one for cell surface staining and the other for
932 permeabilization and whole cell staining.
933 For surface staining, 100 µL of EV or Tspan12+FZD4+LRP5 transfected cells were plated into 6
934 wells of a 96-well v-bottom plates (Costar) and spun down at 300g, for 3 min, (4°C) washed with
935 150 µL cold PBS. In triplicate, EV or Tspan12+FZD4+LRP5 were double-stained with an anti-M2-
936 FLAG antibody conjugated to Alexa Fluor-488 (2 µg/mL) and an anti-Tspan12 antibody
937 conjugated to Alexa Fluor-647 for 30 minutes on ice and protected from light. Control samples,
938 also in triplicate, were incubated with HBS + 2% BSA under the same conditions. After incubation,
939 cells were spun down and washed twice with PBS before final suspension in 100 µL of cold PBS.
940 For permeabilized cell staining, 100 µL of EV or Tspan12+FZD4+LRP5 transfected cells were
941 plated into 6 wells on a 96-well v-bottom plates (Costar) and then spun down at 300g, for 3 min
942 (4°C) and washed with 150 µL cold PBS. We then resuspended and fixed the cells in 100 µL PBS
943 + 1 mM $CaCl_2$ + 0.01% Formaldehyde while slowly shaking for 15 minutes at RT. This was
944 followed by two rounds of 100 µL PBS washes and then permeabilization with 100 µL of PBS +
945 0.5% Tween-20 while slowly shaking for 15 minutes at RT. After two PBS washes, EV or
946 Tspan12+FZD4+LRP5 were double-stained with an anti-M2-FLAG antibody conjugated to Alexa
947 Fluor-488 (2 µg/mL) and an anti-Tspan12 antibody conjugated to Alexa Fluor-647 for 30 minutes
948 on ice and protected from light, in triplicate. Control samples, also in triplicate, were incubated
949 with HBS + 2% BSA under the same conditions. After incubation, the cells were spun down and
950 washed twice with PBS before being resuspended in 100 µL of cold PBS. Fluorescence was
951 analyzed on an Agilent Novocyte 3000. Live/dead gates were set using SSC-A versus FSC-A and

952 singlet gates using FSC-H versus FSC-A, and fluorescence intensity in the 488 and 647 channels
953 was recorded in the doubly gated population.

954
955
956 **REFERENCES**
957

958 1. B. T. MacDonald, K. Tamai, X. He, Wnt/β-Catenin Signaling: Components, Mechanisms,
959 and Diseases. *Dev. Cell* **17**, 9–26 (2009).

960 2. G. Schulte, V. Bryja, The Frizzled family of unconventional G-protein-coupled receptors.
961 *Trends Pharmacol. Sci.* **28**, 518–525 (2007).

962 3. P. Bhanot, *et al.*, A new member of the frizzled family from Drosophila functions as a
963 Wingless receptor. *Nature* **382**, 225–230 (1996).

964 4. C. E. Dann, *et al.*, Insights into Wnt binding and signalling from the structures of two
965 Frizzled cysteine-rich domains. *Nature* **412**, 86–90 (2001).

966 5. C. Y. Janda, D. Waghray, A. M. Levin, C. Thomas, K. C. Garcia, Structural Basis of Wnt
967 Recognition by Frizzled. *Science* **337**, 59–64 (2012).

968 6. K. Tamai, *et al.*, LDL-receptor-related proteins in Wnt signal transduction. *Nature* **407**, 530–
969 535 (2000).

970 7. H.-C. Wong, *et al.*, Direct Binding of the PDZ Domain of Dishevelled to a Conserved
971 Internal Sequence in the C-Terminal Region of Frizzled. *Mol. Cell* **12**, 1251–1260 (2003).

972 8. J. Bilic, *et al.*, Wnt induces LRP6 signalosomes and promotes dishevelled-dependent LRP6
973 phosphorylation. *Science* **316**, 1619–1622 (2007).

974 9. E. Y. Rim, H. Clevers, R. Nusse, The Wnt Pathway: From Signaling Mechanisms to
975 Synthetic Modulators. *Annu. Rev. Biochem.* **91**, 571–598 (2022).

976 10. A. Wodarz, R. Nusse, MECHANISMS OF WNT SIGNALING IN DEVELOPMENT. *Annu.*
977 *Rev. Cell Dev. Biol.* **14**, 59–88 (1998).

978 11. Z. Y. Chen, *et al.*, Isolation and characterization of a candidate gene for Norrie disease. *Nat.*
979 *Genet.* **1**, 204–208 (1992).

980 12. W. Berger, *et al.*, Isolation of a candidate gene for Norrie disease by positional cloning. *Nat.*
981 *Genet.* **1**, 199–203 (1992).

982 13. J. Ke, *et al.*, Structure and function of Norrin in assembly and activation of a Frizzled 4–
983 Lrp5/6 complex. *Genes Dev.* **27**, 2305–2319 (2013).

984 14. A. Meindl, *et al.*, Norrie disease is caused by mutations in an extracellular protein
985 resembling C-terminal globular domain of mucins. *Nat. Genet.* **2**, 139–143 (1992).

986 15. C. Niehrs, The complex world of WNT receptor signalling. *Nat. Rev. Mol. Cell Biol.* **13**,
987 767–779 (2012).

988 16. Q. Xu, *et al.*, Vascular development in the retina and inner ear: control by Norrin and
989 Frizzled-4, a high-affinity ligand-receptor pair. *Cell* **116**, 883–895 (2004).

990 17. X. Ye, Y. Wang, J. Nathans, The Norrin/Frizzled4 signaling pathway in retinal vascular
991 development and disease. *Trends Mol. Med.* **16**, 417–425 (2010).

992 18. K. Nikopoulos, *et al.*, Overview of the mutation spectrum in familial exudative
993 vitreoretinopathy and Norrie disease with identification of 21 novel variants in FZD4,
994 LRP5, and NDP. *Hum. Mutat.* **31**, 656–666 (2010).

995 19. L.-Y. Jia, K. Ma, Novel Norrie disease gene mutations in Chinese patients with familial
996 exudative vitreoretinopathy. *BMC Ophthalmol.* **21**, 84 (2021).

997 20. H. J. Junge, *et al.*, TSPAN12 Regulates Retinal Vascular Development by Promoting Norrin-
998 but Not Wnt-Induced FZD4/β-Catenin Signaling. *Cell* **139**, 299–311 (2009).

999 21. H. T. Maecker, S. C. Todd, S. Levy, The tetraspanin superfamily: molecular facilitators.
1000 *FASEB J.* **11**, 428–442 (1997).

1001 22. M. E. Hemler, Tetraspanin functions and associated microdomains. *Nat. Rev. Mol. Cell Biol.*
1002 **6**, 801–811 (2005).

1003 23. K. J. Susa, A. C. Kruse, S. C. Blacklow, Tetraspanins: structure, dynamics, and principles of
1004 partner-protein recognition. *Trends Cell Biol.* **34**, 509–522 (2024).

1005 24. R. Oren, S. Takahashi, C. Doss, R. Levy, S. Levy, TAPA-1, the target of an antiproliferative
1006 antibody, defines a new family of transmembrane proteins. *Mol. Cell. Biol.* **10**, 4007–4015
1007 (1990).

1008 25. D T Fearon, and R. H. Carter, The CD19/CR2/TAPA-1 Complex of B Lymphocytes:
1009 Linking Natural to Acquired Immunity. *Annu. Rev. Immunol.* **13**, 127–149 (1995).

1010 26. E. Dornier, *et al.*, TspanC8 tetraspanins regulate ADAM10/Kuzbanian trafficking and
1011 promote Notch activation in flies and mammals. *J. Cell Biol.* **199**, 481–496 (2012).

1012 27. R. Nishiuchi, *et al.*, Potentiation of the ligand-binding activity of integrin α3β1 via
1013 association with tetraspanin CD151. *Proc. Natl. Acad. Sci. U. S. A.* **102**, 1939–1944 (2005).

1014 28. L. Liu, *et al.*, Tetraspanin CD151 Promotes Cell Migration by Regulating Integrin
1015 Trafficking. *J. Biol. Chem.* **282**, 31631–31642 (2007).

1016 29. J. A. Poulter, *et al.*, Mutations in TSPAN12 Cause Autosomal-Dominant Familial Exudative
1017 Vitreoretinopathy. *Am. J. Hum. Genet.* **86**, 248–253 (2010).

1018 30. J. A. Poulter, *et al.*, Recessive Mutations in TSPAN12 Cause Retinal Dysplasia and Severe
1019 Familial Exudative Vitreoretinopathy (FEVR). *Invest. Ophthalmol. Vis. Sci.* **53**, 2873–2879
1020 (2012).

1021 31. H. Yang, X. Xiao, S. Li, G. Mai, Q. Zhang, Novel TSPAN12 mutations in patients with
1022 familial exudative vitreoretinopathy and their associated phenotypes. *Mol. Vis.* **17**, 1128–
1023 1135 (2011).

1024 32. Y. Ju, *et al.*, Mutations in TSPAN12 gene causing familial exudative vitreoretinopathy. *Hum.*
1025 *Genomics* **18**, 22 (2024).

1026 33. H. Kondo, *et al.*, Mutations in the *TSPAN12* Gene in Japanese Patients with Familial
1027 Exudative Vitreoretinopathy. *Am. J. Ophthalmol.* **151**, 1095-1100.e1 (2011).

1028 34. M. B. Lai, *et al.*, TSPAN12 Is a Norrin Co-receptor that Amplifies Frizzled4 Ligand
1029 Selectivity and Signaling. *Cell Rep.* **19**, 2809–2822 (2017).

1030 35. H. J. Junge, *et al.*, TSPAN12 Regulates Retinal Vascular Development by Promoting Norrin-
1031 but Not Wnt-Induced FZD4/β-Catenin Signaling. *Cell* **139**, 299–311 (2009).

1032 36. K. Knoblich, *et al.*, Tetraspanin TSPAN12 regulates tumor growth and metastasis and
1033 inhibits β-catenin degradation. *Cell. Mol. Life Sci.* **71**, 1305–1314 (2014).

1034 37. E. S. Bruguera, J. P. Mahoney, W. I. Weis, The co-receptor Tetraspanin12 directly captures
1035 Norrin to promote ligand-specific β-catenin signaling. *eLife* **13**, RP96743 (2025).

1036 38. K. J. Susa, S. Rawson, A. C. Kruse, S. C. Blacklow, Cryo-EM structure of the B cell co-
1037 receptor CD19 bound to the tetraspanin CD81. *Science* **371**, 300–305 (2021).

1038 39. M. A. Skiba, *et al.*, Antibodies expand the scope of angiotensin receptor pharmacology. *Nat.*
1039 *Chem. Biol.* **20**, 1577–1585 (2024).

1040 40. N. Tsutsumi, *et al.*, Structure of human Frizzled5 by fiducial-assisted cryo-EM supports a
1041 heterodimeric mechanism of canonical Wnt signaling. *eLife* **9**, e58464 (2020).

1042 41. J. Jumper, *et al.*, Highly accurate protein structure prediction with AlphaFold. *Nature* **596**,
1043 583–589 (2021).

1044 42. J. Xiang, *et al.*, Successful Strategies to Determine High-Resolution Structures of GPCRs.
1045 *Trends Pharmacol. Sci.* **37**, 1055–1069 (2016).

1046 43. S. Mukherjee, *et al.*, Synthetic antibodies against BRIL as universal fiducial marks for
1047 single−particle cryoEM structure determination of membrane proteins. *Nat. Commun.* **11**,
1048 1598 (2020).

1049 44. J. Ereño-Orbea, *et al.*, Structural Basis of Enhanced Crystallizability Induced by a Molecular
1050 Chaperone for Antibody Antigen-Binding Fragments. *J. Mol. Biol.* **430**, 322–336 (2018).

1051 45. J. Abramson, *et al.*, Accurate structure prediction of biomolecular interactions with
1052 AlphaFold 3. *Nature* **630**, 493–500 (2024).

1053 46. X. Zhang, S. Dong, F. Xu, Structural and Druggability Landscape of Frizzled G Protein-
1054 Coupled Receptors. *Trends Biochem. Sci.* **43**, 1033–1046 (2018).

1055 47. S. Yang, *et al.*, Crystal structure of the Frizzled 4 receptor in a ligand-free state. *Nature* **560**,
1056 666–670 (2018).

1057 48. Y. Qian, *et al.*, Structural basis of Frizzled 4 in recognition of Dishevelled 2 unveils
1058 mechanism of WNT signaling activation. *Nat. Commun.* **15**, 7644 (2024).

1059 49. F.-L. Hsieh, T.-H. Chang, Antibody Display of cell surface receptor Tetraspanin12 and
1060 SARS-CoV-2 spike protein. [Preprint] (2021). Available at:
1061 https://www.biorxiv.org/content/10.1101/2021.05.29.446300v1 [Accessed 25 June 2025].

1062 50. C. H. Lipper, E. D. Egan, K.-H. Gabriel, S. C. Blacklow, Structural basis for membrane-
1063 proximal proteolysis of substrates by ADAM10. *Cell* S009286742300733X (2023).
1064 https://doi.org/10.1016/j.cell.2023.06.026.

1065 51. M. Landau, *et al.*, ConSurf 2005: the projection of evolutionary conservation scores of
1066 residues on protein structures. *Nucleic Acids Res.* **33**, W299–W302 (2005).

1067 52. I. Bang, *et al.*, Biophysical and functional characterization of Norrin signaling through
1068 Frizzled4. *Proc. Natl. Acad. Sci.* **115**, 8787–8792 (2018).

1069 53. F. Berditchevski, E. Odintsova, Tetraspanins as Regulators of Protein Trafficking. *Traffic* **8**,
1070 89–96 (2007).

1071 54. T. Shoham, *et al.*, The Tetraspanin CD81 Regulates the Expression of CD19 During B Cell
1072 Development in a Postendoplasmic Reticulum Compartment. *J. Immunol.* **171**, 4062–4072
1073 (2003).

1074 55. B. Zimmerman, *et al.*, Crystal Structure of a Full-Length Human Tetraspanin Reveals a
1075 Cholesterol-Binding Pocket. *Cell* **167**, 1041-1051.e11 (2016).

1076 56. K. J. Susa, T. C. Seegar, S. C. Blacklow, A. C. Kruse, A dynamic interaction between CD19
1077 and the tetraspanin CD81 controls B cell co-receptor trafficking. *eLife* **9**, e52337 (2020).

1078 57. R. Umeda, *et al.*, Structural insights into tetraspanin CD9 function. *Nat. Commun.* **11**, 1–11
1079 (2020).

1080 58. D. El Mazouni, P. Gros, Cryo-EM structures of peripherin-2 and ROM1 suggest multiple
1081 roles in photoreceptor membrane morphogenesis. *Sci. Adv.* **8**, eadd3677 (2022).

1082 59. J. Ke, *et al.*, Structure and function of Norrin in assembly and activation of a Frizzled 4–
1083 Lrp5/6 complex. *Genes Dev.* **27**, 2305–2319 (2013).

1084 60. C.-F. Bowin, *et al.*, WNT stimulation induces dynamic conformational changes in the
1085 Frizzled-Dishevelled interaction. *Sci. Signal.* **16**, eabo4974 (2023).

1086 61. L. A. Stoddart, *et al.*, Application of BRET to monitor ligand binding to GPCRs. *Nat.*
1087 *Methods* **12**, 661–663 (2015).

1088 62. T.-H. Chang, *et al.*, Structure and functional properties of Norrin mimic Wnt for signalling
1089 with Frizzled4, Lrp5/6, and proteoglycan. *eLife* **4**, e06554.

1090 63. C. Zhang, *et al.*, Norrin-induced Frizzled4 endocytosis and endo-lysosomal trafficking
1091 control retinal angiogenesis and barrier function. *Nat. Commun.* **8**, 16050 (2017).

1092 64. H. Hirai, K. Matoba, E. Mihara, T. Arimori, J. Takagi, Crystal structure of a mammalian
1093 Wnt–frizzled complex. *Nat. Struct. Mol. Biol.* **26**, 372–379 (2019).

1094 65. T.-H. Chang, *et al.*, Structure and functional properties of Norrin mimic Wnt for signalling
1095 with Frizzled4, Lrp5/6, and proteoglycan. *eLife* **4**, e06554 (2015).

1096 66. G. Shen, *et al.*, Structural basis of the Norrin-Frizzled 4 interaction. *Cell Res.* **25**, 1078–1081
1097 (2015).

1098 67. R. L. YAUCH, M. E. HEMLER, Specific interactions among transmembrane 4 superfamily
1099 (TM4SF) proteins and phosphoinositide 4-kinase. *Biochem. J.* **351**, 629–637 (2000).

1100 68. X. A. Zhang, A. L. Bontrager, M. E. Hemler, Transmembrane-4 Superfamily Proteins
1101 Associate with Activated Protein Kinase C (PKC) and Link PKC to Specific β1 Integrins*.
1102 *J. Biol. Chem.* **276**, 25005–25013 (2001).

1103 69. M. Zuidscherwoude, *et al.*, Tetraspanin microdomains control localized protein kinase C
1104 signaling in B cells. *Sci. Signal.* **10**, eaag2755 (2017).

1105 70. C. Y. Logan, R. Nusse, THE WNT SIGNALING PATHWAY IN DEVELOPMENT AND
1106 DISEASE. *Annu. Rev. Cell Dev. Biol.* **20**, 781–810 (2004).

1107 71. F. Bucher, *et al.*, Antibody-Mediated Inhibition of Tspan12 Ameliorates Vasoproliferative
1108 Retinopathy Through Suppression of β-Catenin Signaling. *Circulation* **136**, 180–195
1109 (2017).

1110 72. M. Eubelen, *et al.*, A molecular mechanism for Wnt ligand-specific signaling. *Science* **361**,
1111 eaat1178 (2018).

1112 73. L. J. Bailey, *et al.*, Locking the Elbow: Improved Antibody Fab Fragments as Chaperones for
1113 Structure Determination. *J. Mol. Biol.* **430**, 337–347 (2018).

1114 74. D. N. Mastronarde, Automated electron microscope tomography using robust prediction of
1115 specimen movements. *J. Struct. Biol.* **152**, 36–51 (2005).

1116 75. A. Punjani, J. L. Rubinstein, D. J. Fleet, M. A. Brubaker, cryoSPARC: algorithms for rapid
1117 unsupervised cryo-EM structure determination. *Nat. Methods* **14**, 290–296 (2017).

1118 76. A. Punjani, H. Zhang, D. J. Fleet, Non-uniform refinement: adaptive regularization improves
1119 single-particle cryo-EM reconstruction. *Nat. Methods* **17**, 1214–1221 (2020).

1120 77. T. C. Terwilliger, S. J. Ludtke, R. J. Read, P. D. Adams, P. V. Afonine, "Improvement of
1121 cryo-EM maps by density modification" (Biochemistry, 2019).

1122 78. R. Sanchez-Garcia, *et al.*, DeepEMhancer: a deep learning solution for cryo-EM volume
1123 post-processing. *Commun. Biol.* **4**, 874 (2021).

1124 79. P. Emsley, B. Lohkamp, W. G. Scott, K. Cowtan, Features and development of Coot. *Acta*
1125 *Crystallogr. D Biol. Crystallogr.* **66**, 486–501 (2010).

1126 80. E. F. Pettersen, *et al.*, UCSF ChimeraX: Structure visualization for researchers, educators,
1127 and developers. *Protein Sci. Publ. Protein Soc.* **30**, 70–82 (2021).

1128 81. P. D. Adams, *et al.*, PHENIX: a comprehensive Python-based system for macromolecular
1129 structure solution. *Acta Crystallogr. D Biol. Crystallogr.* **66**, 213–221 (2010).

1130 82. P. V. Afonine, *et al.*, Real-space refinement in PHENIX for cryo-EM and crystallography.
1131 *Acta Crystallogr. Sect. Struct. Biol.* **74**, 531–544 (2018).

1132 83. C. J. Williams, *et al.*, MolProbity: More and better reference data for improved all-atom
1133 structure validation. *Protein Sci. Publ. Protein Soc.* **27**, 293–315 (2018).

1134 84. B. A. Barad, *et al.*, EMRinger: side chain-directed model and map validation for 3D cryo-
1135 electron microscopy. *Nat. Methods* **12**, 943–946 (2015).

1136 85. A. Morin, *et al.*, Collaboration gets the most out of software. *eLife* **2**, e01456 (2013).

1137